Journal
of
The Franklin Institute
Devoted to Science and the Mechanic Arts

Vol. 269 MAY, 1960 No. 5

OUR UNBALANCED BIAD *

BY

CHAUNCEY D. LEAKE [1]

The title of my talk, "Our Unbalanced Biad," contains a word not to be found in our dictionaries. You may, nevertheless, realize quickly what I am to talk about, when I suggest that there are two arms to our intellectual balance. Part of our continuing job of learning is to keep these long arms of intellectual effort in balance—the humanities on the one hand and the sciences on the other.

In our time we are condensing the long respected Greek triad of logics, ethics and aesthetics into the biad of the sciences and the humanities. Are we wise? Is the balancing of our scientific disciplines with our humanistic studies to be enough?

THE GREEK TRIAD

One may find existential relations between the concepts of logics, ethics and aesthetics. In order to gain satisfactions in living, it is necessary first to find somewhat of what we call the "truth" about ourselves and the universe surrounding us. This is the business of logics.

In the light of such knowledge as we acquire, we are then prepared to examine the motives which determine our conduct and our relations with other people, in seeking the goals we prefer in our hierarchy of values. Here is the problem for ethics.

Then comes the question of how best to apply our knowledge to the achievement of our purposes, to reach the satisfactions we crave. This is the function of aesthetics.

---

* Address delivered at the Annual Meeting of The Franklin Institute on Wednesday, January 20, 1960.

[1] President, American Association for the Advancement of Science; Professor of Pharmacology, The Ohio State University, Columbus, Ohio.

(Note—The Franklin Institute is not responsible for the statements and opinions advanced by contributors in the JOURNAL.)

In our current terminology, the logics have become our sciences, the aesthetics our arts. What has happened to the ethics? Have these evaporated into our "value judgments," or are they condensed with our arts into the "humanities"?

Many ways of obtaining truth have been tried, from oriental emphasis on subjective experience, including mystical revelation, to occidental preoccupation with objective observation. Aristotle's great achievement was to systematize principles of reasoning. His deductive formal logic became so powerful that it was *the* logic, so that the word itself was used only in the singular. Aristotelianism dominated occidental intellectual affairs for centuries. It was brilliantly exploited by the Christian Fathers, and became the foundation of scholasticism.

Other forms of logic were not revived until recently. Inductive logic, frequently used in the natural sciences, grew with the Renaissance. A logic of science, with verifiability by measuring, gradually evolved. Symbolic logic has developed with mathematics. Other non-Aristotelian logics are being explored.

Interestingly, modern neurophysiology is confirming psychoanalytical insight by finding analogical processes associated with coding mechanisms in the functioning of our brains. These seem to be prime in creativity. Analogy involves recognition of potential relationships between what has hitherto been conventionally thought to be unrelated. Free association, or free conscious analogy, may be the greatest stimulus to creativity in both the arts and sciences. Its honest use may itself free us from our stereotyped conventionalities.

The great merit of the scientific method is that verification by reference to agreed-upon standards of measurement establishes a basis for agreement on what constitutes the "truth." It is interesting how the psychological factor of voluntary agreement becomes paramount in science. Even the standards used for measuring have validity merely by agreement.

It is this verifiability that assures the strength of modern science. However, in our naive awe at this enormously powerful tool, let us remember that wisdom is more than verifiable and agreed-upon knowledge of ourselves and our environment. There still remain the problems of what to use this knowledge for, and how best to use it for the purposes we may agree upon.

In approaching the ethical problem, the ancient Greeks saw the conflict between conduct directed toward self-gratification on the one hand, and the welfare of society on the other. The relation of individuals to the societies in which they live remains vastly complicated with uncountable and ever-changing factors. Yet both old and new democracies depend on *voluntary* agreement among the people in a community as to appropriate goals toward which they might willingly work together.

The aesthetic problem involves judgment in choice of the most fitting or appropriate way by which our agreed-upon (or scientific) knowledge of ourselves and our environment can be applied to the accomplishment of our agreed-upon purposes. Judgment is sharpened only by practice or experience, as every artist or engineer or physician learns. A successful aesthetic solution calls for discerning taste in the fitness or propriety of things or ideas. Voluntary social agreement is more difficult to obtain in aesthetics than in logics or ethics, and when it is reached, there tends to be conventionalization, with status stratification.

The triadic relationship among logics, ethics and aesthetics is mediated by the neglected factor of voluntary agreement, and may be expressed in terms of objectives: the function of logics is to establish truth; the goal of ethics is to obtain good; and the purpose of aesthetics is to achieve beauty. The true, the good, and the beautiful thus comprise a trinity which retains its appeal and its power. There seems to be an indication that the truth itself points toward that which is good and beautiful.

The Greek triad, relating logics, ethics and aesthetics, probably reached its clearest expression in the 5th Century B.C. under the influence of Plato. Thinkers have played variations on the theme ever since. By no means have we fully explored its capabilities or its significance. Peculiarly, in our critical time, we are attempting to alter the stability of this triad, and perhaps foolishly to simplify it.

269
50

THE CURRENT BIAD

Slowly, imperceptively, almost unconsciously, our academic trend, which sets the direction of our intellectual life, has narrowed the traditional triad of logics, ethics and aesthetics to the current biad of the sciences and the humanities. Significantly, and perhaps to our woe, ethics seem either to have dropped out of social consideration, or to be somehow or other included among the humanities.

Our age of science is a time of crisis. Our value judgments are in chaos. Old values are weak and new ones uncertain. Many of our cherished beliefs are being shaken by the rough demonstrable facts about ourselves and our universe. Yet it is part of our scientific spirit, as my revered teacher, Edwin Grant Conklin, emphasized, to be confident that unwanted truth is better than cherished error. Here is a supreme value judgment.

Our occidental culture has withstood many crises. The ancient myths, now being so entertainingly examined by Robert Graves, may record the overthrow of matriarchal societies with the growth of patrilineal tribes, as human males realized that they had something to do with continuing the race. Later legends indicate the decline of nature worship in the face of a vigorous Greek rationality, which in turn deteriorated under Roman luxury and administrative rigidity. Population pressures destroyed the materialistic stability of the Caesarean world, and into the darkness came a yearning faith in spiritual reward, which crystallized in an authoritarianism built on absolute ideals.

The great Thomistic achievement in the 13th Century of a solid faith corresponding precisely with then demonstrable fact began to crack as the alleged facts were questioned by a skeptical humanism. Copernican theory, extended by Kepler, toppled the cosmology of antiquity; Harvey overthrew the neat Galenical system of how our animal bodies work; Galileo, Boyle and Lavoisier shook intellectual complacency with the verifiable measurements that started modern physics and chemistry; Ludwig and Helmholtz issued a manifesto of faith that all living processes are explainable in terms of physics and chemistry, with lasting reverberations in the Russia that became the testing ground for another manifesto; and Darwin roughly disturbed the comfortable religious beliefs of our great-grandparents a century ago.

It is interesting to note how Newton's rigid system of measured checks and balances, which even set a pattern for political and economic doctrine, as reflected in the United States Constitution, should yield first to the concept of gradual change through evolution as introduced by Darwin, and then to the more general idea of relativity as developed by Einstein. It is ironic that now we seem to have come to the certainty of uncertainty!

As we pursue our probing of the world around us, we go from space-time confusion in the tiniest bits of organized energy in nuclear particles to time-space bewilderment in receding nebulae and an unbelievable expanding universe, with infinity compounded by indefiniteness. We find no answer to the riddle of being.

Life itself baffles us. We observe in the macromolecules of genes and viruses no clear dividing line between what lives and what doesn't. We learn, following Virchow's idea of studying disease from cells to societies, that organizational levels of living material involve factors not capable of physical or chemical explanation. Further we discover that we ourselves, in the very act of observing, modify what we observe. The psychology of *gestalt* further breaks down the materialistic mansion we have built and come to fear.

This then is another time of intellectual crisis. It is brought on by the very success of our scientific logic. Planck's quantum theory, with the thermodynamics of Gibbs and Maxwell, and Einstein's mathematical logic, have given us the power of nuclear energy, with a glimpse into the energy factors which may control life itself. The failure of our ethics appears in our distressing dilemma of decision: shall we use nuclear power for arrogant threats in daring mutual destruction, or shall we use it for the peaceful benefit of all people?

Our social schizophrenia can be diagnosed from our aggressive practice in the face of our professed peaceful intent. Effective therapy directed toward bringing into balance the applications of our sciences with the implications of our humanities may depend on sharpening the fulcrum of our self-knowledge. Perhaps Socratic echoes may still stir us.

Our dissatisfactions grow from our anxieties that our generous good-willed ideals of behavior cannot be realized in the crass materialism of a machine-like world. Such anxieties yield to frustrations as we begin to see that we may not get the sort of satisfactions we want. Then our frustrations focus in resentments against those we think are blocking our paths. Thus our scientists are blamed for our manifest distress, and an anti-intellectualism arises. Artistic endeavor becomes unintelligible to the uninitiated; blasé beatniks with their ladies in Levis squawk rebellion; and conventional wisdom calls for more science in the name of security.

Our international and individual crises are produced both by insufficient knowledge, especially of ourselves, and by inability through fear to join voluntarily in social agreements as to common purposes. A psychology of determent emerges, perhaps to stabilize a nobler psychology of responsibility.

OUR LACK OF BALANCE

We are thus beginning to sense our difficulties and our failures. In seeking by scientific means to obtain the truth about ourselves and our environment, we seem to have put too much emphasis on our environment to the neglect of a merciless study of ourselves. In the relationship, then, between ourselves and our environment, we are out of balance.

Lacking directional ethics, we cannot apply our scientific knowledge to purposes we can agree upon as worthy of universal social endeavor. Our science seems to become applied chiefly to making individual and national status symbols. What gadgetry is directed toward cleanliness, comfort and convenience, is well diluted by styling for false-fronting, and the waste is monumental. What profit longer life from medical science if there is so little chance yet for living it with graciousness, dignity, self-confidence and self-reliance? What social value has our science if it is applied so successfully to the possibility of destroying us all?

The social impact of science has been tremendous. We have brought many frightening problems for which we are quite unprepared. Of universal concern are such as: (1) radiation hazards; (2) over-population dangers; (3) harmful pollution of airs and waters; (4) barriers of misunderstanding and distrust resulting from inequalities in the dissemination and appreciation of scientific knowledge; (5) fears of a stereotyped scientific authoritarianism; and (6) industrial uglification.

Many of the applications of our scientific knowledge thus bring further imbalance in our cultural endeavor. If we are to build a balanced biad for measuring the success of our living adventure, we must emphasize the humanities along with the sciences. Our rapidly growing verifiable knowledge about ourselves and our environment must be balanced by an equal growth in wise judgments in the application of this knowledge to the attainment of the good and the beautiful.

Yet even this balance is not enough, for we seem to be drifting without agreed-upon purposes. "All we like sheep have gone astray," and instead of recognizing our individual responsibilities, we wait for someone else to tell us what to do. Like waiting for Godot, we wait for God, not realizing that within us always is our God, who unites us to all that is not us, to all the rest of the universe, of which we are all a part.

Maybe the attempt to build a balanced biad of the sciences and the humanities is not enough. Ethics is lacking to stabilize the balance. At best a balanced biad is in unstable equilibrium: it can so easily get out of balance by a shift in interest either on the scientific or the humanistic side. We crave stability. Perhaps some of the traditions of our culture, such as those nourished at The Franklin Institute, can help in lighting our way. Perhaps we might well give up the idea of maintaining a balanced biad between the sciences and the humanities, and return to the more stable and fundamental Greek concept of the triad of logics, ethics and aesthetics.

This would be to our advantage. We now have a solid basis for logics in the verifiability of science. We have a keen appreciation of aesthetics in humanistic endeavor. We need, however, to reach agreements on appropriate social goals. These may be supplied by ethical studies.

It is regrettable that philosophy and ethics have generally deteriorated in our academic environments during the last half century. This has coincided with the rise of the materialistic applications of our science. We might greatly benefit were philosophical considerations and discussions to come more widely into our daily lives and activities. It is here especially that our liberal arts colleges can show the way, even for our huge state universities.

Perhaps the philosophers are partly at fault. They seem to have developed, quite as scientists and artists have done, a peculiar jargon and vocabulary of their own, which is not understood or comprehended by people generally. Science, art and philosophy cannot flourish in secret. If they are to have meaning for humanity, they must be part of humanity.

THE HOPE FROM UNDERSTANDING

Often in the challenge of an intellectual crisis, despair may take the place of hope and faith. Understanding, however, as Leonardo da Vinci proclaimed, is the basis for love, and in such understanding there may come renewed hope and faith.

As our world-wide communications continue to improve, we may be sure that the traditional aspirations of people everywhere for a better life will push for the balanced triad of logics, ethics and aesthetics: our science will become more widely understood, and as our inherent love of beauty exerts itself, our applications of scientific knowledge may be ever more wisely directed toward social welfare and the good of people. We are witnessing a new resurgence of enthusiasm for understanding science, for achieving worthy purposes in human welfare, and in preserving the natural beauties of our world, even in our increasing industrialization.

COMPARISON OF YIELD CONDITIONS FOR CIRCULAR CYLINDRICAL SHELLS *

BY

ANTONI SAWCZUK [1] AND PHILIP G. HODGE, JR.[2]

ABSTRACT

The yield condition for a rigid-plastic circular cylindrical shell subjected to axially symmetric loading is described in terms of the circumferential hoop stress n and the axial bending moment m. Different yield conditions are obtained depending on whether the shell is of homogeneous or ideal sandwich construction, and on whether the shell material satisfies Tresca's or Mises' yield condition. Previous work has been limited to Tresca's yield condition.

The example of a long shell subjected to a ring of pressure at its midpoint is considered for each of the four shell yield conditions as well as for a simple "limited interaction" approximation. Complete stress and velocity fields are determined, the limit load is found, and the extent of the plastic region is determined. The results are assessed in terms of the theorems of limit analysis.

1. INTRODUCTION

Previous analyses of plastic shell problems have usually started from the premise that the shell material satisfies Tresca's yield condition of maximum shear stress. However, experimental evidence generally indicates that the actual yield condition is a very complex one and that the Mises yield condition of maximum octahedral shearing stress is a somewhat better approximation to it. Therefore, it seems of some interest to investigate a simple shell problem under the hypotheses of various yield conditions and to compare the results.

In addition to considering different material yield conditions, it is also of interest to consider different types of shell construction. Probably the most common type of shell is one of constant thickness with uniform properties across the thickness. However, it is sometimes mathematically convenient to consider an idealized sandwich shell consisting of two ideally thin sheets separated by a core of finite thickness.

The particular problem chosen for consideration is that of a very long circular cylindrical shell, subjected to a single ring load. The shell is assumed to be sufficiently long so that the support conditions at the end are immaterial. In this case, the plastic action is confined to a finite region symmetric about the ring of force. The complete problem

---

* The results presented in this paper were obtained in the course of an investigation sponsored by the Office of Naval Research.

[1] Post-Doctoral Fellow, Illinois Institute of Technology, on leave from the Polish Academy of Sciences, Chicago, Ill.

[2] Professor of Mechanics, Illinois Institute of Technology, Chicago, Ill.

is to determine the extent of this plastic region, the plastic collapse load (the magnitude of the force necessary to cause plastic action), and the stress and velocity distributions throughout the plastic region.

A complete solution of this problem has previously been given (1)[3] for a simplified limited interaction curve[4] which has no direct physical meaning. In addition, the plastic collapse load has been computed for the Tresca yield condition, for both the uniform and sandwich shells (1). The present paper derives the complete stress solutions for the four combinations of yield conditions and shell structure and the velocity solutions for the sandwich shells.

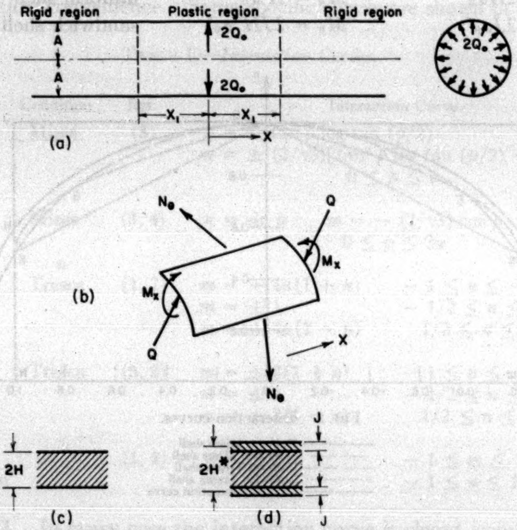

FIG. 1. Cylindrical shell with ring load.

(*a*) Loaded shell
(*b*) Stress resultants
(*c*) Section of uniform shell
(*d*) Section of sandwich shell

Section 2 of this paper gives the basic equations of the problem and the interaction curves for the various theories. A general method of solution is derived in Sec. 3. Section 4 then presents formulas for the various shells considered. Finally, the different solutions are compared in Sec. 5.

---

[3] The boldface numbers in parentheses refer to the references appended to this paper.

[4] So-called because the restrictions on direct force and moment are assumed to be independent of each other.

2. BASIC EQUATIONS

The basic equations of cylindrical shell theory are well known (see, for example, (2)). The problem is defined in terms of the radial velocity W and three stress resultants per unit length: the circumferential direct stress N_θ, the axial moment M_x, and the shear force Q. Sign conventions for the stresses are defined in Fig. 1; W is positive outward. We find it convenient to use the following dimensionless quantities:

$$\begin{array}{llll} n = N_\theta/N_0 & m = M_x/M_0 & w = W/A & \\ q = A^{1/2}(M_0N_0)^{-1/2}Q & & x = N_0^{1/2}(AM_0)^{-1/2}X & \\ N_0 = 2H\sigma_0 & M_0 = H^2\sigma_0 & \text{uniform shell} & \quad (1) \\ N_0 = 2J\sigma_0^* & M_0 = 2JH^*\sigma_0^* & \text{sandwich shell} & \end{array}$$

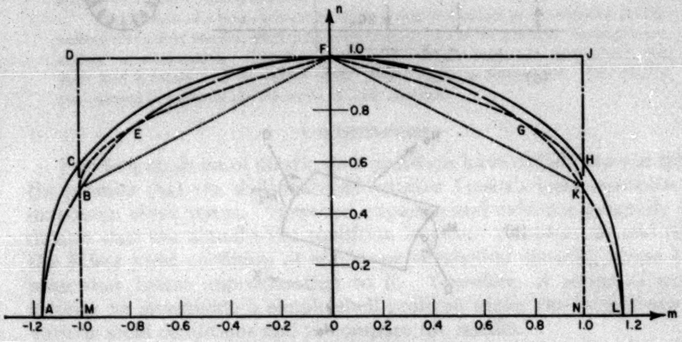

FIG. 2. Interaction curves.

——— Uniform Mises shell
— — — Sandwich Mises shell
- - - - Uniform Tresca shell
·············· Sandwich Tresca shell
—-—-— Limited interaction curve

The coordinate is measured from the point of application of the ring load; primes will be used to represent derivatives with respect to x; σ_0 and σ_0^* are the yield stresses of the uniform shell and sandwich shell materials, respectively; shell dimensions are shown in Fig. 1.

The behavior of a rigid perfectly plastic cylindrical shell is defined by two equilibrium equations, an interaction curve, and a flow law. In dimensionless terms and with no distributed surface loads present, the equilibrium equations are

$$q' + n = 0 \tag{2}$$

$$m' = q. \tag{3}$$

It is assumed that the effect of the shear force on plastic yielding is negligible. Therefore, a description of the plastic behavior can be given in terms of n and m only. It is convenient to give this description in a stress-resultant-space with coordinates n and m.

We begin with the interaction curve which plays the same role in stress-resultant-space as the yield curve in stress-space. Indeed, beginning with a given shell construction (uniform or ideal sandwich) and a given material yield condition (Mises or Tresca), one can derive the corresponding interaction curve in terms of n and m. Alternatively, one may assume the form of interaction curve directly as a property of the integrated shell based, for example, on experimental results or mathematical convenience. Some specific curves are shown in Table I and Fig. 2. In every case the interaction curve is closed, convex, and symmetric with respect to both m and n.

TABLE I.—*Interaction Curves.*

Shell Structure	Condition	Ref.	Interaction Curve	
Uniform	Mises	(3)	$n = \pm \tan p \log \tan (p/2)$ $m = \pm (2/\sqrt{3})[\tan^2 p \log \tan (p/2) + \sec p]$ $0 \leq p \leq \pi$	
Sandwich	Mises	(3, 4)	$n = \sin p \quad m = -(2/\sqrt{3}) \cos p$ $0 \leq p \leq 2\pi$	
Uniform	Tresca	(1, 2)	$m = \mp 4n(1 + n)$ $m = \pm 1$ $m = \pm 4n(1 - n)$	$-1 \leq n \leq -1/2$ $-1/2 \leq n \leq 1/2$ $1/2 \leq n \leq 1$
Sandwich	Tresca	(5, 2)	$m = \pm 2(1 + n)$ $m = \pm 1$ $m = \pm 2(1 - n)$	$-1 \leq n \leq -1/2$ $-1/2 \leq n \leq 1/2$ $1/2 \leq n \leq 1$
Limited Interaction		(1, 2)	$n = \pm 1$ $m = \pm 1$	$-1 \leq m \leq 1$ $-1 \leq n \leq 1$

If the stress point for a particular value of x is within the interaction curve, no plastic flow is possible; thus for our ideal rigid-plastic material the shell is rigid.

If the stress point is on the interaction curve, plastic flow may occur according to the plastic potential flow law. This flow law depends not only upon the state of stress but also upon the assumed interaction curve. Let e_θ and k_x be the dimensionless unit circumferential extension rate and axial curvature rate respectively, of the middle surface of the shell and superpose axes k_x, e_θ on the m, n axes in Fig. 2. The flow law then states that the "strain-rate vector" with components k_x, e_θ

must be directed along the outward normal to the interaction curve at the stress point in question. In terms of the present variables,

$$k_x = w'' \qquad e_\theta = w.$$

Therefore, if dm and dn represent increments along the interaction curve the plastic flow rule states that

$$w''dm + wdn = 0. \tag{4}$$

Finally, since the material does not exhibit strain hardening, the stress point can never lie outside of the interaction curve.

In general, the stress distribution in a rigid-plastic material may not be uniquely determined, but the plastic collapse load is necessarily unique. It follows that the statement of the basic boundary value problem must be carefully made. We are asked to determine four functions m, n, q, and w and a load magnitude q_0 such that the following requirements are all satisfied:

(*a*) Eqs. 2 and 3 are everywhere valid;
(*b*) the stress point (m, n) is everywhere on (plastic) or inside of (rigid) the interaction curve;
(*c*) in a plastic region, Eq. 4 is valid;
(*d*) in a plastic region, the strain rate vector (w'', w) is directed outwards from the interaction curve;
(*e*) in a rigid region, $w = 0$;
(*f*) all stress and velocity boundary conditions are satisfied;
(*g*) the moment m, shear force q, and velocity w are everywhere continuous;
(*h*) the slope w' is continuous except that if m takes on its extreme possible value, w' may have a discontinuity (hinge circle) of the same sign as m.

A physical consideration of the problem suggests that the plastic deformation will be confined to a central portion $-x_1 \leq x \leq x_1$ of the shell and that $n \geq 0$ in this region. Therefore, the boundary conditions for the plastic region are

$$q = q_0 \quad \text{at} \quad x = 0 \tag{5}$$

$$w' = 0 \quad \text{or} \quad m = \text{minimum at } x = 0$$

$$w' = 0 \quad \text{or} \quad m = \text{maximum at } x = x$$

$$w = 0 \quad \text{at} \quad x = x_1. \tag{8}$$

3. GENERAL SOLUTION

To obtain a general solution to the problem defined in Sec. 2, we express all quantities in terms of a parameter p chosen so that $dm/dp \geq 0$. In particular, m and n are known functions of p given by the parametric representation of the interaction curve:

$$m = m(p) \qquad n = n(p). \tag{9}$$

Equations 2 and 3 then become

$$(dq/dp)p' + n = 0 \tag{10a}$$

$$(dm/dp)p' = q. \tag{10b}$$

Elimination of p' from Eqs. 10a and 10b then leads to an equation whose solution can be written

$$q^2 = q_0^2 - 2\int_{p_0}^{p} n(dm/dp)dp. \tag{11}$$

Here p_0 is the value of p at $x = 0$, and the boundary condition (Eq. 5) has been incorporated in the solution.

If q_1 and p_1 denote the values of q and p at $x = x_1$, Eq. 11 can be solved for the collapse load q_0:

$$q_0^2 = q_1^2 + 2\int_{p_0}^{p_1} n(dm/dp)dp. \tag{12}$$

The lower bound theorem of limit analysis (2) states that any stress field which satisfies conditions (a) and (b) and the stress portions of (f) and (g) will provide a lower bound on the collapse load. Assuming, for the moment, that the stress field can be continued into the rigid region, any choice of p_0, p_1 and q_1 will provide a lower bound on q_0. Holding q_1 fixed and noting that the integrand in Eq. 12 is positive, we see that the highest lower bound is obtained when p_1 is a maximum and p_0 a minimum. This implies that m is a minimum at $x = 0$ and a maximum at $x = x_1$. But if m is a maximum at x_1 and m' is continuous there, $m' = q = q_1 = 0$. Therefore, Eqs. 12 and 11 become

$$q_0 = \left[2\int_{p_0}^{p_1} n(dm/dp)dp\right]^{1/2} \tag{13a}$$

$$q = \left[2\int_{p}^{p_1} n(dm/dp)dp\right]^{1/2} \tag{13b}$$

With q known as a function of p from Eq. 13b, Eq. 10b can be written

$$(dm/dp)(dp/dx) = q$$

and solved explicity for x:

$$x = \int_{p_0}^{p} (1/q)(dm/dp)dp. \tag{13c}$$

In particular, the plastic-rigid boundary is given by

$$x_1 = \int_{p_0}^{p_1} (1/q)(dm/dp)dp. \tag{13d}$$

In general, Eq. 13c must be integrated numerically. Once this has been done, m, n, and q may all be computed as functions of the coordinate x from Eqs. 9 and 13b.

If the shell is sufficiently long, it is evident that some solution of Eqs. 2 and 3 for $x > x_1$ can be found such that the prescribed support conditions at the end of the shell will be satisfied and the stress point will always be on or inside of the interaction curve.[5] Therefore, the proposed solution satisfies all requirements on stresses.

Next, we shall show that a velocity field of the form

$$w = Cq \tag{14}$$

satisfies all requirements on velocity. Indeed, it follows from Eqs. 2 and 3 that

$$\begin{aligned} q''(dm/dp) &= -\, n'(dm/dp) = -\, (dn/dp)p'(dm/dp) \\ &= -\, m'(dn/dp) = -\, q(dn/dp) \end{aligned} \tag{15}$$

so that Eq. 14 satisfies Eq. 4. Further, m is such that the boundary conditions (Eqs. 6 and 7) are satisfied, and Eq. 14 satisfies the boundary condition (Eq. 8). Finally, it follows from Eq. 13b that q, and hence w, is always positive; therefore the strain-rate vector is directed outwards from the top side $n \geq 0$ of the interaction curve.

Therefore, the proposed solution satisfies all of conditions (a–h) and hence our hypothesis is verified.

4. EXAMPLES

We consider first the sandwich shell with Mises' yield condition. The interaction curve in Table I is already in the proper parametric form, and

$$p_0 = 0 \qquad p_1 = \pi. \tag{16}$$

Substituting from Table I and Eqs. 16 into Eqs. 13 we obtain

$$q_0 = (2\pi/\sqrt{3})^{1/2} = 1.905 \tag{17a}$$

$$q = (1/\sqrt{3})[2(\pi - p) + \sin 2p]^{1/2} \tag{17b}$$

---

[5] The question of how long the shell must be and the modification necessary for short shells has been dealt with for a particular interaction curve (2, 6) and will not be considered here.

$$x = 2\cdot 3^{-1/4}\int_0^p \sin p[2(\pi - p) + \sin 2p]^{-1/2}dp \qquad (17c)$$

$$x_1 = 3.467. \qquad (17d)$$

For the uniform shell with Mises' yield condition, the appropriate portion of the interaction curve is given by the lower sign in Table I. Equations 16 are still applicable, so that Eqs. 13 become

$$q_0 = 2^{1/2}\cdot 3^{-3/4}\cdot\pi = 1.949 \qquad (18a)$$

$$\begin{aligned} q = q_0[1 - (2/\pi^2)\{2 \tan^3 p[\log\tan(p/2)]^2 \\ + \tan p \sec p \log\tan(p/2) - \tan p \\ - \int_0^p \sec p \log\tan(p/2)dp\}]^{1/2} \end{aligned} \qquad (18b)$$

$$x = -\frac{4}{\sqrt{3}}\int_0^p \frac{\tan p[\log\tan(p/2) + \cos p]}{q(p)\cos^2 p}dp. \qquad (18c)$$

The numerical value of x_1 was not calculated for this case.

The relevant portion of the interaction curve for the uniform shell with Tresca's yield condition consists of the two arcs *BEF*, *FGK* in Fig. 2. These may be written in parametric form:

$$\left.\begin{aligned} n &= 1 + p \quad & m &= 4p(1 + p) \quad & -1/2 &\leq p \leq 0 \\ n &= 1 - p \quad & m &= 4p(1 - p) \quad & 0 &\leq p \leq 1/2 \end{aligned}\right\} \qquad (19)$$

Therefore, Eqs. 13 lead to

$$q_0 = (10/3)^{1/2} = 1.826 \qquad (20a)$$

$$\left.\begin{aligned} q &= (1/\sqrt{3})(5 - 24p - 36p^2 - 16p^3)^{1/2} \qquad & -1/2 \leq p \leq 0 \\ q &= (1/\sqrt{3})(1 - 2p)(5 - 4p)^{1/2} \qquad & 0 \leq p \leq 1/2 \end{aligned}\right\} \qquad (20b)$$

$$\left.\begin{aligned} x &= 4\sqrt{3}\int_{-1/2}^p (1 + 2p)(5 - 24p - 36p^2 - 16p^3)^{-1/2}dp \qquad & -1/2 \leq p \leq 0 \\ x &= 4\sqrt{3}[0.1818 + \sqrt{5} - (5 - 4p)^{1/2}] \qquad & 0 \leq p \leq 1/2 \end{aligned}\right\} \qquad (20c)$$

$$x_1 = 2.379. \qquad (20d)$$

For the sandwich shell with Tresca's yield condition, the pertinent part of the interaction curve is the broken line *BFK* in Fig. 2. This maybe written parametrically in the form

$$\left.\begin{aligned} n &= 1 + p \quad & m &= 2p \quad & -1/2 &\leq p \leq 0 \\ n &= 1 - p \quad & m &= 2p \quad & 0 &\leq p \leq 1/2 \end{aligned}\right\} \qquad (21)$$

Substitution of Eqs. 21 into Eqs. 13 then furnishes the results

$$q_0 = \sqrt{3} = 1.732 \tag{22a}$$

$$\begin{aligned} q &= (1/\sqrt{2})(3 - 8p - 4p^2)^{1/2} & -1/2 \le p \le 0 \\ q &= (1/\sqrt{2})(3 - 8p + 4p^2)^{1/2} & 0 \le p \le 1/2 \end{aligned} \tag{22b}$$

$$\begin{aligned} x &= \sqrt{2}\sin^{-1}[2(p+1)/\sqrt{7}] & -1/2 \le p \le 0 \\ x &= 2.532 - \sqrt{2}\cosh^{-1} 2(1-p) & 0 \le p \le 1/2 \end{aligned} \tag{22c}$$

$$x_1 = 2.532. \tag{22d}$$

Finally, for the limited interaction curve, the relevant portion can be written

$$n = 1 \qquad m = p \qquad -1 \le p \le 1 \tag{23}$$

so that Eqs. 13 become

$$q_0 = 2 \tag{24a}$$

$$q = (2 - 2p)^{1/2} \tag{24b}$$

$$x = 2 - (2 - 2p)^{1/2} \tag{24c}$$

$$x_1 = 2. \tag{24d}$$

The complete results for the limited interaction curve and some of the results for the Tresca yield condition were previously obtained by Drucker (1).

TABLE II.—*Comparison of Collapse Loads.*

		1	2	3	4	5
			Difference from	Difference, %		
Shell Structure	Yield Condition	q_0	Uniform Mises	Actual	Lower Bound	Upper Bound
Uniform	Mises	1.949	0	0	0	0
Sandwich	Mises	1.905	−0.044	−2.3	−2.3	2.6
Uniform	Tresca	1.826	−0.123	−6.3	−6.3	7.9
Sandwich	Tresca	1.732	−0.217	−11.1	−11.1	5.7
Limited Interaction		2.000	0.051	2.6	−20.0	18.2
Elastic ($\nu = 0.3$)		1.289	−0.660	−33.8	—	—

5. COMPARISON OF RESULTS

We discuss first the collapse loads predicted by the various theories. For the sake of argument, we assume that the uniform shell with Mises' yield condition represents the actual problem to be solved, and that all other theories are to be regarded as approximate ones. The first column of Table II collects the collapse loads from Sec. 4, the second column shows the differences from the actual collapse load, and column three shows the percentage difference.

In view of the lower bound theorem of limit analysis (2), if the collapse load is computed according to two interaction curves, one of which lies wholly interior to the other, the collapse load according to the interior curve is necessarily smaller than the other. It follows immediately from Fig. 2 that the collapse load for any problem computed for the sandwich Mises, uniform Tresca, or sandwich Tresca shell is a lower bound on the actual collapse load.

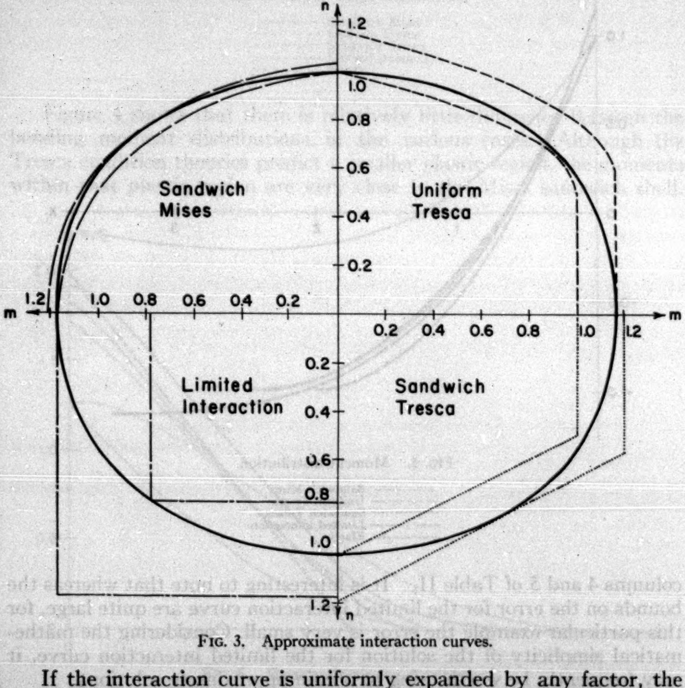

FIG. 3. Approximate interaction curves.

If the interaction curve is uniformly expanded by any factor, the corresponding collapse load will be multiplied by the same factor since the dimensioned collapse load is directly proportional to the yield stress. If, for example, we expand the interaction curve for the uniform Tresca shell by a factor of $2/\sqrt{3} = 1.155$, the new collapse load will be (1.155)

(1.826) = 2.108. However, as shown in the first quadrant of Fig. 3, such an expansion results in a curve wholly exterior to the actual one. Therefore, 2.108 is an upper bound on the actual collapse load. In other words, by considering only the uniform Tresca shell, we can obtain both lower and upper bounds on the uniform Mises shell.

Similar reasoning can be applied to each of the other approximate interaction curves. The various quadrants of Fig. 3 show the other curves scaled to be interior and exterior to the curve for the uniform Mises shell. The resulting bounds, shown as percentage differences from the actual collapse load of the uniform Mises shell, are given in columns 4 and 5 of Table II. It is interesting to note that whereas the bounds on the error for the limited interaction curve are quite large, for this particular example the error is very small. Considering the mathematical simplicity of the solution for the limited interaction curve, it may frequently be worth using to obtain approximate solutions.

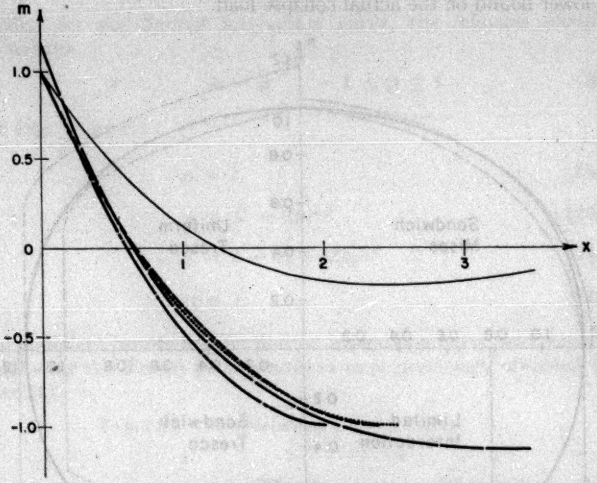

FIG. 4. Moment distribution.

Comparisons of the stress and velocity solutions are made in Figs. 4, 5 and 6. In each case, the quantities are plotted at the corresponding collapse load.

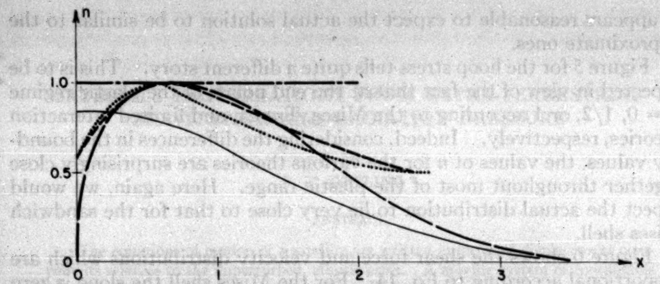

FIG. 5. Hoop stress distribution.

Figure 4 shows that there is relatively little difference between the bending moment distributions in the various cases. Although the Tresca condition theories predict a smaller plastic region, the moments within that plastic region are very close to the Mises sandwich shell.

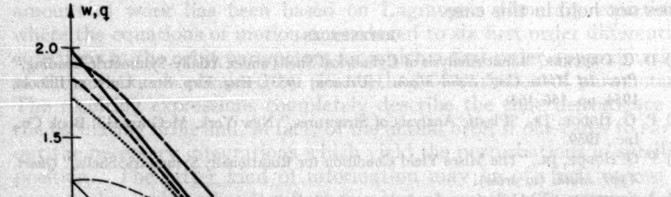

FIG. 6. Shear and velocity distribution.

It appears reasonable to expect the actual solution to be similar to the approximate ones.

Figure 5 for the hoop stress tells quite a different story. This is to be expected in view of the fact that at the end points of the plastic regime $n = 0$, $1/2$, or 1 according to the Mises, Tresca, and limited interaction theories, respectively. Indeed, considering the differences in the boundary values, the values of n for the various theories are surprisingly close together throughout most of the plastic range. Here again, we would expect the actual distribution to lie very close to that for the sandwich Mises shell.

Figure 6 shows the shear force and velocity distributions which are proportional according to Eq. 14. For the Mises shell the slope is zero at $x = 0$ and $x = x_1$, whereas there are hinge circles of discontinuous slope according to the other theories. Despite this difference in end conditions, the resulting deformed shapes are very similar through most of the plastic region.

For comparative purposes, the elastic solution at the maximum elastic load is also shown in Figs. 4, 5, and 6. It is qualitatively quite different from the plastic solutions. This difference indicates that a considerable stress redistribution takes place during the stage of contained plastic deformation. In Fig. 6, of course, the elastic curves for shear force and velocity are quite different from each other since Eq. 14 does not hold in this case.

REFERENCES

(1) D. C. DRUCKER, "Limit Analysis of Cylindrical Shells under Axially-Symmetric Loading," *Proc. 1st Midw. Conf. Solid Mech.* (Urbana, 1953), Eng. Exp. Sta., Univ. of Illinois, 1954, pp. 158–163.

(2) P. G. HODGE, JR., "Plastic Analysis of Structures," New York, McGraw-Hill Book Co., Inc., 1959.

(3) P. G. HODGE, JR., "The Mises Yield Condition for Rotationally Symmetric Shells," *Quart. Appl. Math.* (in press).

(4) A. SAWCZUK, "Yield Surfaces for Anisotropic Shells," (to be published).

(5) P. G. HODGE, JR., "The Rigid-Plastic Analysis of Symmetrically Loaded Cylindrical Shells," *J. Appl. Mech.*, Vol. 21, pp. 336–342 (1954).

(6) G. EASON AND R. T. SHIELD, "The Influence of Free Ends on the Load Carrying Capacities of Cylindrical Shells," *J. Mech. Phys. Solids*, Vol. 4, pp. 17–27 (1955).

SATELLITE PERTURBATIONS FROM EXTRA-TERRESTRIAL GRAVITATION AND RADIATION PRESSURE

BY

F. T. GEYLING [1]

ABSTRACT

The equations of motion of a satellite are written in terms of displacement components relative to the unperturbed, elliptic orbit. A moving system of coordinates is used which consists of an orthogonal triad whose origin is always located at the nominal satellite position on the elliptic orbit. This approach differs from the conventional one by way of Lagrange's planetary equations in that the primary results are expressions for the satellite position rather than the osculating orbit elements, which seems an advantage for practical applications. Calculations are carried out for the effects of perturbations in the initial conditions of satellite motion and perturbations due to oblateness, lunar and solar gravitation, and solar radiation pressure. In the numerical examples special attention has been devoted to the performance of a thin mylar balloon acting as a passive communication satellite.

INTRODUCTION

In the field of satellite perturbation analysis by far the largest amount of work has been based on Lagrange's planetary equations where the equations of motion are reduced to six first order differential equations in the orbit parameters for which a first order approximation of the solution is obtained by the method of variation of parameters. The resulting expressions completely describe the time dependence of the osculating orbit and, in fact, of the actual orbit if one cares to carry out the necessary integrations which yield the perturbations in satellite position. The latter kind of information may be of chief interest to space technologists who classify themselves as amateurs by astronomers' standards but who nevertheless need to know where a radar is to be pointed in order to track a vehicle whose motion has been characterized by previous measurements. In particular it should be convenient to know the extent to which the various physical perturbations cause a vehicle to depart from a position that can be forecast by simple elliptic orbit calculations for the unperturbed case. This idea of using an elliptic orbit as a reference is an obvious one and has been carried into a variety of integration schemes such as Hansen's method, but to the present writer's knowledge the existing literature on the motion of satellite vehicles contains very few analytic realizations of this approach.

Specific calculations have been carried out for cases where the nominal, that is, unperturbed, orbit is circular and a generalization of the results to elliptic nominal orbits will be given elsewhere.[2] Since the effects of lunar and solar gravitation as well as radiation pressure are of some current interest in connection with communication satellites, many of the numerical examples have been tailored to this application.

---

[1] Bell Telephone Laboratories Incorporated, Murray Hill, N. J.

1. THE EQUATIONS OF MOTION

For a dynamical system whose Lagrangian has been found, the Hamiltonian is defined as

$$H(p, q, t) = \sum_i \dot{q}_i p_i - L \tag{1}$$

where the generalized momenta are

$$p_i = \frac{\partial L}{\partial \dot{q}_i}. \tag{2}$$

By means of this last relation, the Hamiltonian can be written as a function of q, p, t. The canonical equations of Hamilton are then

$$\dot{q}_i = \frac{\partial H}{\partial p_i}$$

and

$$\dot{p}_i = -\frac{\partial H}{\partial q_i}.$$

One advantage of the Hamiltonian approach to dynamic problems lies in the fact that the Hamiltonian may contain time explicitly, which can be due to a time-dependent coordinate system, time-dependent constraints, or a time-dependent potential function, V, in the Lagrangian. A dynamical system whose H contains t explicitly is said to be rheonomic.

For the present work we find it attractive to select a moving coordinate system whose origin always coincides with the satellite position in unperturbed elliptic motion. This nominal satellite position is O' in Fig. 1 where the plane of the ellipse is inclined by the angle i to the plane x, y. Any perturbations in the initial conditions or on the path will then result in satellite displacements about this point. A solution in this form is obviously convenient in determining satellite positions for tracking purposes. On the other hand one can still calculate secular perturbations for the osculating ellipse such as apsidal, anomalistic, and nodal precessions from these solutions without difficulty. We describe the displacement from O' in terms of u, v, w (Fig. 1) where the u-axis points radially outward from the ellipse, the v-axis at right angles thereto in the plane of the nominal orbit and in the direction of anomalistic motion, and the w-axis normal to that plane according to the right-hand rule.

---

[2] F. T. Geyling and H. R. Westerman, "The Dynamics of Space Vehicles," Reading (Mass.), Addison-Wesley, in preparation.

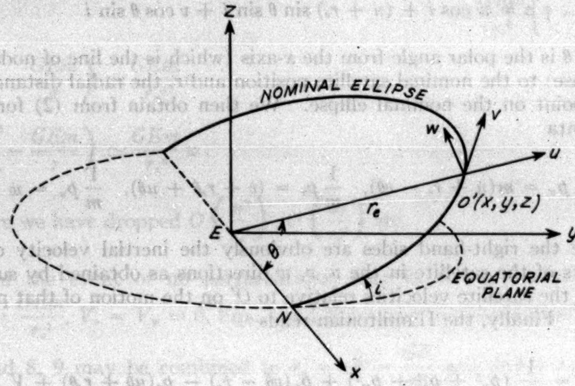

FIG. 1.

In the x, y, z system of coordinates of Fig. 1 we have for the kinetic and potential energy of the moving body

$$T = \frac{m}{2}\left(\dot{x}^2 + \dot{y}^2 + \dot{z}^2\right)$$

and

$$V = \frac{GEm}{r} + \tilde{V}$$

where

m = mass of satellite
E = mass of Earth
G = universal gravitational constant
$r = [x^2 + y^2 + z^2]^{1/2}$
$\tilde{V}$ = whatever perturbative potential is being considered in addition to the first term in V, which of course represents a spherical Earth.[3]

Dots indicate time derivatives.

---

[3] A theorem of Poincare's shows that for small perturbations the law of superposition holds, that is, various physical effects may be considered individually and their effects on satellite motion superimposed to describe the resultant orbit.

According to the procedure which was just outlined, we first express T and V in terms of u, v, w by the relations

$$\begin{aligned} x &= (u + r_e)\cos\theta - v\sin\theta \\ y &= -w\sin i + (u + r_e)\sin\theta\cos i + v\cos\theta\cos i \\ z &= w\cos i + (u + r_e)\sin\theta\sin i + v\cos\theta\sin i \end{aligned}$$

where θ is the polar angle from the x-axis (which is the line of nodes in this case) to the nominal satellite position and r_e the radial distance to that point on the nominal ellipse. We then obtain from (2) for the momenta

$$\frac{1}{m}p_u = m(\dot{u} + \dot{r}_e - v\dot{\theta}), \quad \frac{1}{m}p_v = (\dot{v} + r_e\dot{\theta} + u\dot{\theta}), \quad \frac{1}{m}p_w = \dot{w} \qquad (3)$$

(where the right-hand sides are obviously the inertial velocity components of the satellite in the u, v, w directions as obtained by superposing the satellite velocities relative to O' on the motion of that point itself). Finally, the Hamiltonian reads

$$H = \frac{1}{2m}(p_u^2 + p_v^2 + p_w^2) + p_u(v\dot{\theta} - \dot{r}_e) - p_v(u\dot{\theta} + r_e\dot{\theta}) + V \qquad (4)$$

and Hamilton's equations for this problem are

$$\dot{p}_u = \dot{\theta}p_v - V_u \qquad (5)$$

$$\dot{p}_v = -\dot{\theta}p_u - V_v \qquad (6)$$

$$\dot{p}_w = -V_w \qquad (7)$$

$$\dot{u} = \frac{1}{m}p_u + v\dot{\theta} - \dot{r}_e \qquad (8)$$

$$\dot{v} = \frac{1}{m}p_v - u\dot{\theta} - r_e\dot{\theta} \qquad (9)$$

$$\dot{w} = \frac{1}{m}p_w. \qquad (10)$$

The terms V_u, V_v, and V_w represent partial derivatives of the total potential $V = -\dfrac{GEm}{r} + \tilde{V}$ with respect to u, v, w. Since

$$r = [(r_e + u)^2 + v^2 + w^2]^{1/2}$$

V. 19

we have

$$\frac{\partial}{\partial u}\left(-\frac{GEm}{r}\right) = \frac{GEm}{r_e^3}(r_e + u)\left[1 - \frac{3u}{r_e} + O\left(\frac{u^2, v^2, w^2, \cdots}{r_e^2}\right)\right]$$

$$\simeq \frac{GEm}{r_e^2}\left[1 - 2\frac{u}{r_e}\right]$$

$$\frac{\partial}{\partial v}\left(-\frac{GEm}{r}\right) \simeq \frac{GEm}{r_e^3}v$$

$$\frac{\partial}{\partial w}\left(-\frac{GEm}{r}\right) \simeq \frac{GEm}{r_e^3}w$$

where we have dropped $O\left(\frac{u^2}{r_e^2}\right)$, $O\left(\frac{uv}{r_e^2}\right)$ etc.

In the event of no perturbations, that is, $u = v = w \equiv 0$ and $V_u = \frac{GEm}{r_e^2}$, $V_v = V_w \equiv 0$, Eqs. 7 and 10 become trivial whereas Eqs. 5, 6 and 8, 9 may be combined to $\ddot{r}_e = r_e\dot{\theta}^2 - \frac{GE}{r_e^2}$ and $2\dot{r}_e\dot{\theta} + r_e\ddot{\theta} = 0$. These we recognize as the equations for conic-section orbits, which are satisfied by r_e according to definition. Therefore we drop all terms from Eqs. 3 to 10 which contain r_e but not u, v, w. We may then make use of the fact that

$$\frac{d}{dt} = \frac{\partial}{\partial\theta}\dot{\theta}$$

and

$$\dot{\theta} = [GEa(1 - e^2)]^{1/2}/r_e^2$$

where

a = the semimajor axis, and

e = the eccentricity of the nominal orbit.

Elimination of p_u, p_v, p_w from Eqs. 5 to 10 then yields

$$u'' - 2v' - u - 2[u + e(u' - v)\sin(\theta - \theta_p)]/[1 + e\cos(\theta - \theta_p)]$$

$$= -\frac{a^3(1 - e^2)^3}{GEm}\tilde{V}_u/[1 + e\cos(\theta - \theta_p)]^4 \quad (11)$$

$$v'' + 2u' - v - [-v + 2e(v' + u)\sin(\theta - \theta_p)]/[1 + e\cos(\theta - \theta_p)]$$

$$= -\frac{a^3(1 - e^2)^3}{GEm}\tilde{V}_v/[1 + e\cos(\theta - \theta_p)]^4 \quad (12)$$

$$w'' + [w - 2w'e \sin(\theta - \theta_p)]/[1 + e\cos(\theta - \theta_p)]$$
$$= -\frac{a^3(1-e^2)^3}{GEm}\,\bar{V}_w/[1 + e\cos(\theta - \theta_p)]^4 \quad (13)$$

where primes denote differentiation with respect to θ, and θ_p denotes the central angle from node to perigee of the nominal orbit.

At this point we make the nominal orbit circular, whereby $e = 0$ and $a = r_c$, the constant radius of the nominal orbit. For the independent variable we shall sometimes write $\theta = \theta_0 + f$ where $f = 0$ at $t = t_0$, the starting time of the solution, and θ_0 locates the moving origin O' at this instant (see Fig. 3). Equations 11 to 13 now reduce to

$$u'' - 2v' - 3u = -\frac{r_c^3}{GEm}\,\bar{V}_u \quad (14)$$

$$v'' + 2u' = -\frac{r_c^3}{GEm}\,\bar{V}_v \quad (15)$$

$$w'' + w = -\frac{r_c^3}{GEm}\,\bar{V}_w. \quad (16)$$

2. SOLUTIONS FOR THE RELATIVE MOTION

Equations 14 to 16 may now be readily solved in the homogeneous and the inhomogeneous forms. In the first case we have the solutions

$$u = \frac{2}{\dot\theta}\dot{v}_0 + 4u_0 - \left(\frac{2}{\dot\theta}\dot{v}_0 + 3u_0\right)\cos f + \frac{1}{\dot\theta}\,\dot{u}_0 \sin f \quad (17)$$

$$v = v_0 - \frac{2}{\dot\theta}\,\dot{u}_0 - 3\left(\frac{1}{\dot\theta}\dot{v}_0 + 2u_0\right)f + 2\left(\frac{2}{\dot\theta}\dot{v}_0 + 3u_0\right)$$
$$\times \sin f + \frac{2}{\dot\theta}\,\dot{u}_0 \cos f \quad (18)$$

$$w = \frac{1}{\dot\theta}\,\dot{w}_0 \sin f + w_0 \cos f \quad (19)$$

where $\dot\theta = \left(\frac{GE}{r_c^3}\right)^{1/2}$. These solutions are of course dependent on the initial conditions for their magnitude and we shall show their application to orbit calculations in the next section. At present we use them to generate particular solutions of Eqs. 14 to 16 by a straightforward application of the method of variation of parameters. The results are

$$
\begin{aligned}
u = \frac{r_c^3}{mGE}\Big[-2\int \tilde{V}_v df + 2\cos f\int \tilde{V}_v \cos f\, df \\
+ \cos f\int \tilde{V}_u \sin f\, df + 2\sin f\int \tilde{V}_v \sin f\, df \\
- \sin f\int \tilde{V}_u \cos f\, df\Big]
\end{aligned}
\tag{20}
$$

$$
\begin{aligned}
v = \frac{r_c^3}{mGE}\Big[3\int\int \tilde{V}_v df\, df + 2\int \tilde{V}_u df - 4\sin f\int \tilde{V}_v \cos f\, df \\
- 2\sin f\int \tilde{V}_u \sin f\, df + 4\cos f\int \tilde{V}_v \sin f\, df \\
- 2\cos f\int \tilde{V}_u \cos f\, df\Big]
\end{aligned}
\tag{21}
$$

$$
w = \frac{r_c^2}{mGE}\Big[\cos f\int \tilde{V}_w \sin f\, df - \sin f\int \tilde{V}_w \cos f\, df\Big] \tag{22}
$$

where all integrals are left indefinite for the time being.

3. PERTURBATIONS OF THE INITIAL CONDITIONS

As was mentioned in Section 2, solutions 17 to 19 represent the satellite's motion relative to the circular orbit if at $t = t_0$ some set of displacements and velocities u_0, v_0, w_0, and $\dot{u}_0$, $\dot{v}_0$, $\dot{w}_0$ relative to the circular orbit exist. These may be errors in the ballistic launch, occurring at t_0, or observational errors in a sighting which takes place at t_0 and from which the orbit is to be predicted. Equations 17 to 19 then exhibit the changes of the orbit due to these perturbations in the initial conditions and may be used to obtain expressions for the so-called orbit sensitivities.[4]

Since Eqs. 17 to 19 represent deviations of the satellite from the circular path, it should be pointed out that the expression for $r_c + u$ represents indeed an elliptic orbit of small eccentricity. We note that the perturbations of initial conditions in a nonrotating coordinate system are related to u and v by $\Delta V = v_0 + u_0\dot{\theta}$ and $\dot{r} = \dot{u}_0$ where ΔV and $\dot{r}$ are the horizontal and vertical velocity errors at cut-off. Solving for $\dot{v}_0$ and $\dot{u}_0$ from these relations and substituting into Eq. 17 yield

$$
u = \frac{2\Delta V}{\dot{\theta}} + 2\Delta r - \left(\frac{2\Delta V}{\dot{\theta}} + \Delta r\right)\cos f + \frac{\dot{r}}{\dot{\theta}}\sin f. \tag{23}
$$

---

[4] This particular application of moving coordinates to perturbations in the initial conditions has indeed been made previously by A. D. Wheelon in Lecture 12B of a joint course on space technology by the University of California and the Space Technology Laboratories in 1958.

The same result may be obtained by writing the equation of an elliptic orbit in terms of its dynamic parameters and expanding for small e.

We have

$$r = \frac{c_1^2/GE}{1 + e\cos(f - f_p)} \simeq \frac{c_1^2}{GE}[1 - e\cos f\cos f_p - e\sin f\sin f_p] \qquad (24)$$

where

$$\begin{aligned} c_1 &= (V + \Delta V)(r_c + \Delta r), \\ \cos f_p &= [(r_c + \Delta r)(V + \Delta V)^2 - GE]/GEe, \\ \sin f_p &= -(r_c + \Delta r)(V + \Delta V)\dot{r}/GEe, \end{aligned}$$

and f_p locates perigee from θ_0. Substituting these expressions into Eq. 24, we obtain $r = r_c + u$ as with Eq. 23.

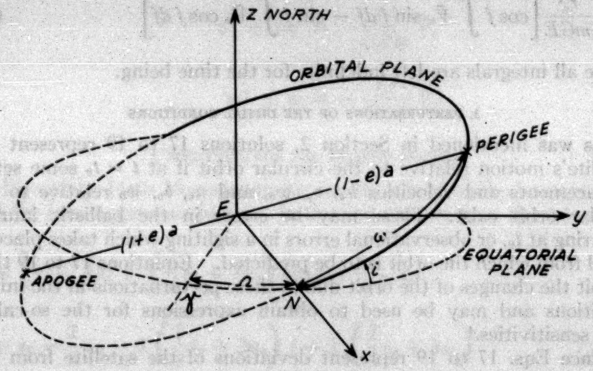

FIG. 2.

Before proceeding to the orbit sensitivities, we note that the complete set of orbit parameters besides a and e, which have already been defined, includes

Ω = the nodal angle between N and γ (see Fig. 2), where the node N is the point at which the satellite crosses the equatorial plane from south to north and γ denotes the first point of Aries as a fixed star reference in the equatorial plane,
i = the orbital inclination,
ω = the angle from node to perigee in the orbital plane (P denoting perigee) where $\omega = \theta_0 + f_p$, and
T_N = the time of nodal passage or "epoch."

One now finds it informative to observe the changes produced in these parameters by the solution u, v, w.

The effect of w is to change the location and the orientation of the orbital plane. By inspection of Fig. 2 one finds from the geometry at the node

$$\Delta\Omega = -\frac{w(-\theta_0)}{\sin i} = \frac{1}{\sin i}\left[\frac{1}{\dot\theta}\,\dot w_0 \sin\theta_0 - w_0 \cos\theta_0\right] \tag{25}$$

and

$$\Delta i = \frac{1}{r_c}\,w'(-\theta_0) = \frac{1}{r_c}\left[\frac{1}{\dot\theta}\,\dot w_0 \cos\theta_0 + w_0 \sin\theta_0\right]. \tag{26}$$

The effects of u, v are of course restricted to changes in orbit shape and timing. The orbit attains its apogee at $u_{\max}$ and its perigee at $u_{\min}$. These two points, marking the line of apsides, are seen to lie at

$$f_{p,a} = \tan^{-1} - \frac{\dot u_0}{(2\dot v_0 + 3\dot\theta u_0)}. \tag{27}$$

If $2\dot v_0 + 3\dot\theta u_0 > 0$, a positive $\dot u_0$ will put the line of apsides into the 2nd and 4th quadrants of f and a negative $\dot u_0$ will put it into the 1st and 3rd quadrants. Some inspection of the geometry of an ellipse in polar coordinates will show that perigee occurs in quadrants 1 and 4 and apogee in 2 and 3. With $2\dot v_0 + 3\dot\theta u_0 < 0$ the situation is reversed. For $2\dot v_0 + 3\dot\theta u_0 = 0$ the line of apsides remains always at right angles to θ_0, where $f_p = \mp\frac{\pi}{2}$ for $\dot u_0 \gtrless 0$. For the maximum and minimum radial excursions from the circle we find

$$u_{\substack{\max\\ \min}} = \frac{2}{\dot\theta}\,\dot v_0 + 4u_0 \pm \frac{1}{\dot\theta}\left[(2\dot v_0 + 3\dot\theta u_0)^2 + \dot u_0^2\right]^{1/2}$$

from which

$$\Delta a = \frac{2}{\dot\theta}\,\dot v_0 + 4u_0 \tag{28}$$

and

$$e = \frac{1}{\dot\theta r_c}\left[(2\dot v_0 + 3\dot\theta u_0)^2 + \dot u_0^2\right]^{1/2}. \tag{29}$$

As should be expected, Δa is independent of $\dot u_0$, that is, insensitive to a nonhorizontal ballistic launch. In the solution for v the term v_0 represents an error committed in the original observation of the polar angle θ_0 which carries over unchanged into all predictions of passage times and is of no further interest. The secular term in Eq. 18 leads to an increment of the satellite's anomalistic period

$$\Delta T_A = -\frac{v(2\pi)}{\dot{\theta} r_c} = \frac{6\pi}{\dot{\theta}^2 r_c}(\dot{v}_0 + 2\dot{\theta} u_0).$$

It is again worth noting that also ΔT_A is unaffected by $\dot{u}_0$. The prediction error for the time of nodal passage is

$$\begin{aligned}\Delta T_N &= -\frac{v(2n\pi - \theta_0)}{\dot{\theta} r_c} \\ &= -\frac{1}{\dot{\theta}^2 r_c}[\dot{\theta} v_0 - 2\dot{u}_0 - 3(\dot{v}_0 + 2\dot{\theta} u_0)(2n\pi - \theta_0) \\ &\qquad - 2(2\dot{v}_0 + 3\dot{\theta} u_0)\sin\theta_0 + 2\dot{u}_0 \cos\theta_0] \qquad (30)\end{aligned}$$

where n is the number of the revolution for which the epoch is to be determined.

Another use may be made of Eqs. 17 to 19 in designing the corrective thrusts required for a satellite rendezvous. Suppose a supply vehicle has been brought into the vicinity of some installation that is already in orbit and the maneuver of homing in on the target has yet to be performed. One may look upon the motion of the cargo ship as a time-varying displacement relative to the target of the form of Eqs. 17 to 19. Four sets of readings of the displacement vector $\vec{\chi}(u, v, w)$ taken by the cargo ship relative to the target at four different points of the target orbit will furnish the constants in Eqs. 17 to 19. At a suitable instant of time t_1, one may then apply the velocity increment $-\frac{\vec{\chi}_1}{\Delta t}$ and follow this up with a second impulse, $+\frac{\chi_1}{\Delta t} - \vec{\chi}_1$, at the time $t_1 + \Delta t$ where Δt is of negligible magnitude compared with the orbital period.

4. PERTURBATIONS BY THE EQUATORIAL BULGE

The well-understood problem of oblateness perturbations shall serve as a test case by which to appraise the present method for treating nonhomogeneous cases. It is customary to make a first approximation to the figure of the Earth by introducing the potential

$$\tilde{V} = -\frac{J r_e^2 G E m}{[(r_e + u)^2 + v^2 + w^2]^{3/2}}\left\{\frac{1}{3} - \frac{z^2}{[(r_c + u)^2 + v^2 + w^2]}\right\} \qquad (31)$$

where r_e shall now denote the Earth's equatorial radius and J is a numerical constant. We then find that

V.2
196

$$\left.\begin{aligned} \tilde{V}_u &= \frac{Jr_c^2GEm}{r_c^4}(1 - 3\sin^2\theta\sin^2 i), \\ \tilde{V}_v &= \frac{Jr_c^2GEm}{r_c^4}\sin 2\theta\sin^2 i, \quad \text{and} \\ \tilde{V}_w &= \frac{Jr_c^2GEm}{r_c^4}\sin 2i\sin\theta. \end{aligned}\right\} \tag{32}$$

In these expressions we have set $[(r_c + u)^2 + v^2 + w^2]^{1/2} \cong r_c$ and $z \simeq r_c \sin\theta \sin i$ after the differentiations. Insertion of Eq. 32 into Eqs. 20 to 22 yields

$$\left.\begin{aligned} u &= \frac{Jr_e^2}{r_c}[-1 + \sin^2 i(\tfrac{3}{2} + \tfrac{1}{6}\cos 2\theta)] \\ v &= \frac{Jr_e^2}{r_c}[(2 - 3\sin^2 i)f + \tfrac{1}{12}\sin^2 i\sin 2\theta] \\ w &= \frac{Jr_e^2}{2r_c}\sin 2i[f\cos\theta - \tfrac{1}{2}\sin\theta]. \end{aligned}\right\} \tag{33}$$

The aperiodic terms in u and v are indeed part of the particular solution and reflect the increase of global mass due to the equatorial bulge.

If we strive for a circular orbit of prescribed size and period, apart from the periodic perturbations due to the equatorial bulge, we encounter certain difficulties in realizing this orbit by suitable corrections of the ballistic launch conditions. Let us denote the total perturbations due to oblateness and launch by $\bar{u}$, $\bar{v}$, $\bar{w}$. Then

$$\bar{u}_0 = u_0 + \frac{Jr_e^2}{r_c}[-1 + \sin^2 i(\tfrac{3}{2} + \tfrac{1}{6}\cos 2\theta_0)] \tag{34}$$

$$v_0 = v_0 + \frac{Jr_e^2}{12r_c}\sin^2 i\sin 2\theta_0 \tag{35}$$

$$\dot{\bar{u}}_0 = \dot{u}_0 - \frac{\dot{\theta}Jr_e^2}{3r_c}\sin^2 i\sin 2\theta_0 \tag{36}$$

$$\dot{\bar{v}}_0 = \dot{v}_0 + \frac{\dot{\theta}Jr_e^2}{r_c}[2 + \sin^2 i(-3 + \tfrac{1}{6}\cos 2\theta_0)]. \tag{37}$$

The constant term in $\bar{u}$ may be written

$$\Delta r_c = \frac{Jr_e^2}{r_c}[-1 + \tfrac{3}{2}\sin^2 i] + \frac{2}{\dot{\theta}}\dot{v}_0 + 4u_0 \tag{38}$$

and the coefficients of the secular term in $\bar{v}$ as

$$\frac{r_c \Delta\theta}{f} = \frac{J r_e^2}{r_c} (2 - 3 \sin^2 i) - 3 \left(\frac{1}{\dot{\theta}} v_0 + 2 u_0 \right). \tag{39}$$

We may set $\bar{v}_0 = \dot{u}_0 = 0$ right away, thereby imposing conditions on v_0 and $\dot{u}_0$ which do not interfere with any of the other equations. If we are trying to realize a predesigned orbit, we should certainly wish to have the mean values of r and θ agree with the specifications and therefore demand that the right-hand sides of Eqs. 38 and 39 vanish. Unfortunately, these equations are not algebraically independent in $\dot{v}_0$ and u_0. We may adopt one or the other and then take Eq. 34 or 37 as an additional condition.

If the emphasis is on an orbit of the correct mean radius, we may take $\Delta r_c = 0$ and $\bar{u}_0 = 0$ where the latter condition calls for cut-off at nominal radius. Solving Eqs. 34 and 38 for u_0 and $\dot{v}_0$ and substituting the results into Eqs. 37 and 39 we obtain

$$\dot{\bar{v}}_0 = \frac{\dot{\theta} J r_e^2}{r_c} \left[-1 + \sin^2 i \left(\tfrac{3}{2} + \tfrac{5}{6} \cos 2\theta_0 \right) \right] = \Delta V \tag{40}$$

and

$$\Delta\dot{\theta} = \frac{\dot{\theta} J r_e^2}{r_c^2} \left[\tfrac{1}{2} - \tfrac{3}{4} \sin^2 i \right]. \tag{41}$$

If on the other hand we take $\Delta\dot{\theta} = 0$ and

$$\Delta V = \dot{\bar{v}}_0 + \bar{u}_0 \dot{\theta} = 0,$$

we obtain

$$u_0 = \frac{J r_e^2}{r_c} \left[\tfrac{2}{3} + \sin^2 i \left(-1 + \tfrac{1}{2} \cos 2\theta_0 \right) \right] \tag{42}$$

and

$$\Delta r_c = \frac{J r_e^2}{r_c} \left[\tfrac{1}{3} - \tfrac{1}{2} \sin^2 i \right]. \tag{43}$$

Equations 40 and 42 vanish only for certain combinations of i and θ_0 while $\Delta r_c = \Delta\dot{\theta} = 0$ for $i = \sin^{-1} \sqrt{\tfrac{2}{3}}$.

Since the $\sin \theta$ term of w in Eq. 33 represents a perturbation on i, we may use Eq. 19 to eliminate it. The resulting corrections for the ballistic launch are

$$\bar{w} = 0$$

and

$$\dot{\bar{w}}_0 = \frac{\dot{\theta} J r_e^2}{2 r_c} \sin 2i \cos \theta_0. \tag{44}$$

As a numerical example let us take $r_e = 5000$ statute miles, $i = 51°$, and $\theta_0 = 50°$. Then Eqs. 40 to 44 yield $\Delta V = -4.37$ ft/sec, $\Delta\dot{\theta} = 4.23\ 10^{-8}$ rad/sec, $\bar{u}_0 = 245$ ft, $\Delta r_e = 858$ ft, and $\dot{w}_0 = 7.65$ ft/sec.

The periodic terms of u and v in Eq. 33 have the double angle 2θ as their argument because of the biaxial symmetry of the force field produced by the equatorial bulge in the orbital plane. Since the attraction from the bulge acts in opposite directions on the northern and the southern halves of the orbit, the simple argument θ is to be expected in the periodic terms of w. The term $f\cos\theta$ in w indicates a precession of the orbital plane and the nodal regression is found from $\Delta w = [w]_{\theta=0}^{\theta=2\pi}$ as

$$\dot{\Omega} = -\frac{\Delta w}{\sin i}\frac{(GE)^{1/2}}{2\pi r_e^{3/2}} = -\left(\frac{GE}{r_e^7}\right)^{1/2} J r_e^2 \cos i$$

which agrees with the results obtained by other methods and amounts to $5.80\ 10^{-7}$ rad/sec or $T_\Omega = 125$ days for the nodal period of a 5000-mile orbit with $i = 51°$. Finally one notes that the complete expressions for u, v, w with the initial conditions adjusted as above furnish a convenient means for predicting satellite positions throughout the orbit. The maximum amplitudes of the periodic perturbations impressed on a nominal orbit of 5000-mile radius are approximately 7000 ft.

V.269
1960

5. PERTURBATIONS BY EXTRA-TERRESTRIAL MASSES

For a study of gravitational perturbations by the moon or sun we locate the perturbing body P in the x, y plane where the latter does not in general have to contain the equator. The central angle $\bar{\theta} = \bar{\theta}_0 + \lambda f$ locates P in the x, y plane in a fashion analogous to the way in which O' was located in the orbital plane (Fig. 3). $\bar{\theta}$ is measured from the positive x-axis. $\bar{\theta}_0$ is its initial value at $t = f = 0$ and λ is the ratio between the angular velocity of P and the satellite. We note that the present problem will be rheonomic not only because of the time-dependent u, v, w coordinate system but also due to a time-dependent perturbing potential resulting from the motion of P. λ will be $\ll 1$ in all cases of practical interest.

If one writes the perturbing potential as

$$\tilde{V} = -mGP\left[\frac{1}{R_{pm}} - \frac{xx_p + yy_p + zz_p}{R_p^3}\right]$$

where x_p, y_p, z_p are the coordinates of P, $R_p^2 = x_p^2 + y_p^2 + z_p^2$, and $R_{pm}^2 = (x_p - x)^2 + (y_p - y)^2 + (z_p - z)^2$ then one finds for the perturbative acceleration of the satellite in the x-direction

$$\ddot{\tilde{x}} = -\frac{1}{m}\frac{\partial\tilde{V}}{\partial x} = GP\left[\frac{x_p - x}{R_{pm}^3} - \frac{x_p}{R_p^3}\right]$$

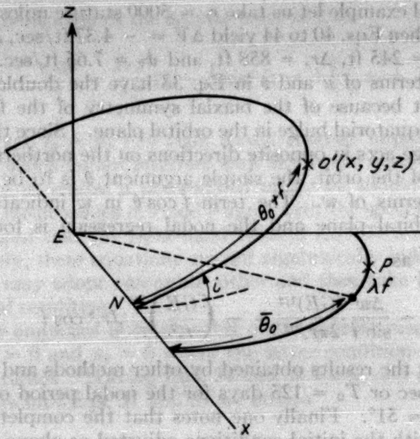

FIG. 3.

which is the sum of the direct and indirect perturbations on the satellite. Analogous expressions follow for $\ddot{y}$ and $\ddot{z}$. We use approximations of the type

$$\frac{\partial \tilde{V}}{\partial x} = -\frac{mGP}{R_p{}^3}\left[\frac{3x_p}{R_p{}^3}(xx_p + yy_p + zz_p) - x\right]$$

and take $x \simeq r_e \cos\theta$, $y \simeq r_e \sin\theta \cos i$, $z \simeq r_e \sin\theta \sin i$ in these expressions to obtain

$$\begin{aligned}
\tilde{V}_u &= \sum \frac{\partial \tilde{V}}{\partial x, y, z}\,\frac{\partial x, y, z}{\partial u} \\
&= -\frac{3r_e\dot{G}Pm}{8R_p{}^3}\left[\tfrac{4}{3}\cos^2 i - \tfrac{2}{3}\sin^2 i + 2\sin^2 i\cos 2\theta + 2\sin^2 i \cos 2\bar{\theta}\right. \\
&\qquad \left. + (1-\cos i)^2\cos 2(\bar{\theta}+\theta) + (1+\cos i)^2\cos^2(\bar{\theta}+\theta)\right] \\
\tilde{V}_v &= -\frac{3r_eGPm}{8P_p{}^3}\left[-2\sin^2 i \sin 2\theta\right. \qquad\qquad (45) \\
&\qquad \left. + (1+\cos i)^2 \sin 2(\bar{\theta}-\theta) - (1-\cos i)^2\sin 2(\bar{\theta}+\theta)\right] \\
\tilde{V}_w &= \frac{3r_eGPm}{4R_p{}^3}\left[\sin 2i \sin\theta + (1-\cos i)\sin i \sin(2\bar{\theta}+\theta)\right. \\
&\qquad \left. + (1+\cos i)\sin i\sin(2\bar{\theta}-\theta)\right].
\end{aligned}$$

Executing formulas 20 to 22 one finds

$$u = \bar{g}\Big[-\tfrac{2}{3}(2\cos^2 i - \sin^2 i)$$

$$+ \tfrac{4}{3}\sin^2 i \cos 2\theta + \frac{2}{4\lambda^2 - 1}\sin^2 i \cos 2\bar{\theta}$$

$$+ \frac{(\lambda+2)(1-\cos i)^2}{(\lambda+1)(2\lambda+1)(2\lambda+3)}\cos 2(\bar{\theta}+\theta)$$

$$+ \frac{(\lambda-2)(1+\cos i)^2}{(\lambda-1)(2\lambda-1)(2\lambda-3)}\cos 2(\bar{\theta}-\theta)\Big] \quad (46)$$

$$v = \bar{g}\Big[\tfrac{4}{3}(2\cos^2 i - \sin^2 i)f$$

$$- \tfrac{11}{8}\sin^2 i \sin 2\theta - \frac{2\sin^2 i}{\lambda(4\lambda^2 - 1)}\sin 2\bar{\theta}$$

$$- \frac{(4\lambda^2 + 12\lambda + 11)(1-\cos i)^2}{4(\lambda+1)^2(2\lambda+1)(2\lambda+3)}\sin 2(\bar{\theta}+\theta)$$

$$+ \frac{(4\lambda^2 - 12\lambda + 11)(1+\cos i)^2}{4(\lambda-1)^2(2\lambda-1)(2\lambda-3)}\sin 2(\bar{\theta}-\theta)\Big] \quad (47)$$

$$w = \bar{g}\Big[\tfrac{1}{2}\sin 2i \sin\theta - f\sin 2i\cos\theta$$

$$- \frac{(1-\cos i)\sin i}{2\lambda(\lambda+1)}\sin(2\bar{\theta}+\theta)$$

$$- \frac{(1+\cos i)\sin i}{2\lambda(\lambda-1)}\sin(2\bar{\theta}-\theta)\Big] \quad (48)$$

where $\bar{g} = -\dfrac{3Pr_c^4}{8ER_p^3}$.

This solution is invalid for $\lambda = 0, \pm 1, \pm\frac{1}{2}, \pm\frac{3}{2}$. Treating the case $\lambda = 0$ separately, formulas 20 to 22 yield

$$u = \bar{g}[-\tfrac{2}{3}(2\cos^2 i - \sin^2 i) + \tfrac{4}{3}\sin^2 i\cos 2\theta - 2\sin^2 i\cos 2\bar{\theta}_0$$

$$+ \tfrac{2}{3}(1-\cos i)^2\cos 2(\theta+\bar{\theta}_0) + \tfrac{2}{3}(1+\cos i)^2\cos 2(\theta-\bar{\theta}_0)] \quad (49)$$

$$v = \bar{g}[\tfrac{4}{3}(2\cos^2 i - \sin^2 i + 3\sin^2 i\cos 2\bar{\theta}_0)f - \tfrac{11}{8}\sin^2 i\sin 2\theta$$

$$- \tfrac{11}{12}(1-\cos i)^2\sin 2(\theta+\bar{\theta}_0) - \tfrac{11}{12}(1+\cos i)^2\sin 2(\theta-\bar{\theta}_0)] \quad (50)$$

$$\begin{aligned} w = \bar{g}\Big[&[(1 + \cos i)\sin i \cos(\theta - 2\bar{\theta}_0) \\ &- (1 - \cos i)\sin i \cos(\theta + 2\bar{\theta}_0) - \sin 2i \cos\theta]f \\ &+ \tfrac{1}{2}\sin 2i \sin\theta + \tfrac{1}{2}(1 - \cos i)\sin i \sin(\theta + 2\bar{\theta}_0) \\ &\qquad - \tfrac{1}{2}(1 + \cos i)\sin i \sin(\theta - 2\bar{\theta}_0)\Big]. \end{aligned} \qquad (51)$$

For ease of physical interpretation, we begin with an examination of this case.

If we set $x_p = z_p = 0$, $y_p = R_p$, $\bar{\theta}_0 = \dfrac{\pi}{2}$, $i = 0$, $\theta_0 = 0$, and $f = \theta$ then we have coincidence between the orbital planes of the satellite and the perturbing body; in addition, the latter has been fixed on the positive y-axis and the satellite is assumed to start its motion on the positive x-axis. With these conditions we find

$$\left.\begin{aligned} \tilde{V}_u &= -\frac{3r_cGPm}{2R_p^3}\left[\tfrac{1}{3} - \cos 2\theta\right] \\ V_v &= -\frac{3r_cGPm}{2R_p^3}\sin 2\theta \\ V_w &= 0 \end{aligned}\right\} \qquad (45')$$

and

$$\left.\begin{aligned} u &= \bar{g}\left[-\tfrac{4}{3} - \tfrac{8}{3}\cos 2\theta\right] \\ v &= \bar{g}\left[\tfrac{8}{3}\theta + \tfrac{11}{3}\sin 2\theta\right] \\ w &\equiv 0. \end{aligned}\right\} \qquad (49')$$

The first terms in u and v are due to the first term in $\tilde{V}_u$ of Eq. 45′. The secular term in v, which is to be avoided in the case of a 24-hr satellite, may be eliminated by use of the complementary solutions in a fashion similar to the calculations of Section 4.

The second terms in u and v are consequences of the so-called "tidal effect" of P on the orbit. One notes from u that the orbit elongates in the x-direction and flattens in the y- direction and v reflects the angular anomalies which the satellite must undergo in order to satisfy conditions of angular momentum and energy while its distance from the central mass is continually changing. In fact, these considerations of angular momentum and energy permit an alternate way of analyzing the present, simplified case which will be reproduced here for illustrative reasons.

Figure 4 shows a view of the x, y plane and the forces, due to P, acting on the satellite in its orbit. It can be shown that

$$F_x = -\frac{r_cGPm\cos\theta}{R_p^3}$$

and

$$F_v = \frac{2r_e GPm \sin\theta \cos i}{R_p^3}$$

and thus, with $i = 0$,

$$F_t = \frac{3r_e GPm \sin\theta \cos\theta}{R_p^3}$$

and

$$F_r = \frac{r_e GPm}{R_p^3}[2\sin^2\theta - \cos^2\theta].$$

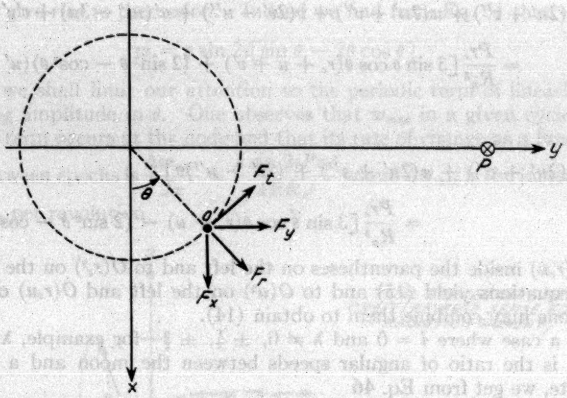

FIG. 4.

We recall that

$$\frac{dK}{dt} = F_t U_t + F_r U_r$$

and

$$\frac{dA}{dt} = F_t(r_e + u) - F_r v$$

where

K = total energy of the satellite in the geocentric frame,
A = angular momentum of the satellite about the Earth,

$$U_r = \dot{u} - v\dot{\theta}$$

and

$$U_t = \dot{\theta}(r_e + u) + \dot{v},$$

the instantaneous geocentric radial and tangential velocities, respectively. From

$$K = \frac{m}{2}\left[[\dot{\theta}(r_c + u) + \dot{v}]^2 + [\dot{u} - v\dot{\theta}]^2\right] - \frac{GEm}{[(r_c + u)^2 + v^2]^{1/2}}$$

and

$$A = m\dot{\theta}[(r_c + u + v')(r_c + u) - (u' - v)v]$$

we obtain after simplification

$$\frac{E}{r_c^3}[r_c(2u' + v'') + u(2u' + v'') + v(2v' - u'') + u'(u'' - 3u) + v'v'']$$
$$= \frac{Pr_c}{R_p^3}[3 \sin\theta \cos\theta(r_c + u + v') + (2\sin^2\theta - \cos^2\theta)(u' - v)]$$

and

$$\frac{E}{r_c^3}[r_c(2u' + v'') + u(2u' + v'') + (2v' - u'')v]$$
$$= \frac{Pr_c}{R_p^3}[3 \sin\theta \cos\theta(r_c + u) - (2\sin^2\theta - \cos^2\theta)v].$$

To $O(r_c u)$ inside the parentheses on the left and to $O(r_c^2)$ on the right, both equations yield (15) and to $O(u^2)$ on the left and $O(r_c u)$ on the right one may combine them to obtain (14).

In a case where $i = 0$ and $\lambda \neq 0, \pm \frac{1}{2}, \pm \frac{3}{2}$—for example, $\lambda \simeq \frac{1}{28}$ which is the ratio of angular speeds between the moon and a 24-hr satellite, we get from Eq. 46

$$\dot{u} = \dot{g}\left[-\frac{4}{3} - \frac{(2 - \lambda)4}{(1 - \lambda)(1 - 2\lambda)(3 - 2\lambda)} \cos 2(1 - \lambda)\theta\right]. \qquad (46')$$

$u_{\min}$ occurs at $\theta = \dfrac{(2n + 1)\pi}{2(1 - \lambda)}, n = 0, 1, 2, \cdots$. As was to be expected, this means that the orbit's minor axis, generated by the tidal effect, rotates in phase with the perturbing body P. The periodic term in v is

$$\dot{g}\,\frac{(4\lambda^2 - 12\lambda + 11)}{(1 - \lambda)^2(1 - 2\lambda)(3 - 2\lambda)} \sin 2(1 - \lambda)\theta$$

which produces maximum circumferential displacements of the satellite at points which are $\dfrac{\pi}{4}$ out of phase with respect to the orbit axes. For $\lambda = \frac{1}{28}$ we find $v_{\max} \simeq 3000$ ft for a 24-hr satellite. If the maximum angular displacement of such a relay must stay within ± 10° for transmission purposes, the periodic term which was just computed is seen to be negligible. If, however, one assumes a typical guidance error of $\dot{v}_0 = \Delta V = 1$ ft/sec during the launch, then the time between corrective tangential impulses for such an installation will be of the order of $\frac{10 r_e \dot{\theta}}{57.3 \dot{v}_0 6\pi} = 93$ days, where we have used Eq. 18.

Let us next consider a case where $i \neq 0$, but $\lambda = 0$ and all other previous conditions are maintained. The tidal distortion of the orbit is now somewhat more involved as can be seen from Eqs. 46 and 47 and may be understood by inspection of the geometry. However, the perturbing body now also exerts a tidal moment on the orbit which should give rise to precession. Indeed we find from Eq. 51 that

$$w = \breve{g} \sin 2i[\sin\theta - 2\theta\cos\theta] \tag{51'}$$

where we shall limit our attention to the periodic term of linearly increasing amplitude in θ. One observes that $w_{\max}$ in a given cycle due to this term occurs at the node and that its rate of change as a function of θ between epochs is $\frac{\Delta w_{\max}}{2\pi} = \frac{3 \sin 2iPr_e^4}{4ER_p^3}$ where $\Delta w_{\max}$ is the increment in $w_{\max}$ per revolution.

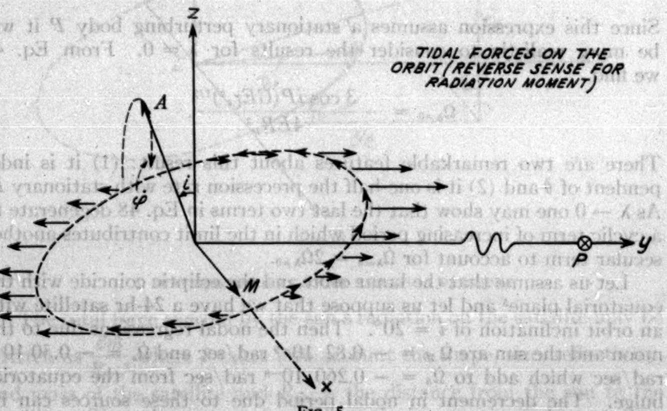
z
TIDAL FORCES ON THE ORBIT (REVERSE SENSE FOR RADIATION MOMENT)
A
i
φ
M
P
y
x

FIG. 5.

On the other hand, arguing again from fundamentals, we have with the help of Fig. 5: $\dot{\varphi} = \frac{M}{A \cos i}$, where M is the average tidal moment exerted on the orbit (positive in the right-hand sense about the x-axis), $\dot{\varphi}$ the average angular rate of orbital precession about the y-axis resulting from this moment (positive in the right-hand sense) and $A = m(GEr_c)^{1/2}$ is the average angular momentum of the satellite. From the geometry at the node we have $w_{\max} = -\dot{\varphi} r_c \cos i$. Now,

$$M = -\frac{1}{2\pi}\int_0^{2\pi}(F_y r_c \sin\theta \sin i - F_z r_c \sin\theta \cos i)d\theta$$

where

$$F_z = -\frac{r_c GPm \sin\theta \sin i}{R_p{}^3},$$

resulting in

$$M = -\frac{3 \sin 2i r_c{}^2 GPm}{4R_p{}^3}.$$

Combining all of the necessary relations, we have

$$\frac{\Delta w_{\max}}{2\pi} = \frac{r_c \cos i}{\dot{\theta}} \frac{1}{m(GEr_c)^{1/2} \cos i} \frac{3 \sin 2i r_c{}^2 GPm}{4R_p{}^3} = \frac{3 \sin 2i r_c{}^4 P}{4ER_p{}^3}.$$

The most relevant effect of this precession, as far as orbit acquisition is concerned, lies in the nodal regression

$$\dot{\Omega}_{\lambda=0} = \frac{\Delta w_{\max}\dot{\theta}}{2\pi \sin i r_c} = -\frac{3 \cos i P(GEr_c{}^3)^{1/2}}{2ER_p{}^3}.$$

Since this expression assumes a stationary perturbing body P it will be more realistic to consider the results for $\lambda \neq 0$. From Eq. 48 we find

$$\dot{\Omega}_{\lambda\neq 0} = -\frac{3 \cos i P(GEr_c{}^3)^{1/2}}{4ER_p{}^3}.$$

There are two remarkable features about this result: (1) it is independent of $\dot{\theta}$ and (2) it is one-half the precession rate with stationary P. As $\lambda \to 0$ one may show that the last two terms in Eq. 48 degenerate to a cyclic term of increasing period which in the limit contributes another secular term to account for $\dot{\Omega}_{\lambda=0} = 2\dot{\Omega}_{\lambda\neq 0}$.

Let us assume that the lunar orbit and the ecliptic coincide with the equatorial plane[5] and let us suppose that we have a 24-hr satellite with an orbit inclination of $i = 20°$. Then the nodal regressions due to the moon and the sun are $\dot{\Omega}_M = -0.82\ 10^{-9}$ rad/sec and $\dot{\Omega}_s = -0.30\ 10^{-9}$ rad/sec which add to $\dot{\Omega}_0 = -0.260\ 10^{-8}$ rad/sec from the equatorial bulge. The decrement in nodal period due to these sources can be written as

$$\Delta T_\Omega = \frac{2\pi(\dot{\Omega}_M + \dot{\Omega}_s)}{\dot{\Omega}_0(\dot{\Omega}_0 + \dot{\Omega}_M + \dot{\Omega}_s)} = -8418 \text{ days}.$$

---

[5] Without this assumption, the orbit inclination with respect to the x, y plane (containing P) would be variable as a result of the equatorial precession.

(T_{Ω} due to oblateness only is 27,956 days.) The decrement in geoperiod (time between successive ascents over the equator)[6] may be written as

$$\Delta T_G = \frac{(\dot{\Omega}_M + \dot{\Omega}_s)2\pi \cos i}{\dot{\theta}^2} = -\ 1.24 \text{ sec}$$

for the moon and sun combined. If a secular perturbation of i due to P were to exist, it would follow from $\dfrac{di}{dt} = \Delta w'(\theta = 0)$ but this is seen from Eq. 51′ to vanish, as should be the case for small rotations of the orbital plane about the y-axis.

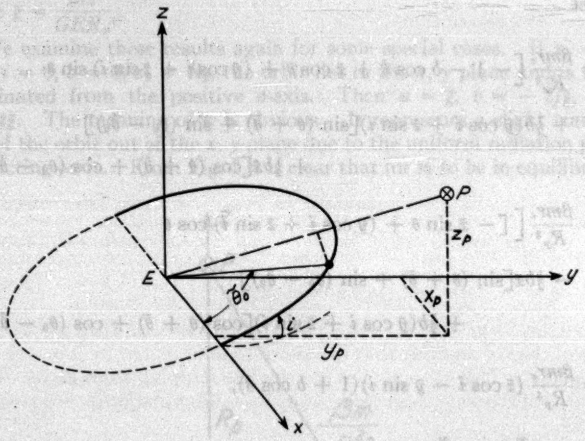

FIG. 6.

6. PERTURBATIONS BY SOLAR RADIATION PRESSURE

The total force exerted by the sun's radiation on the satellite may be written as $\dfrac{\beta m}{R_{pm}{}^2}$ where β takes into account the shape, size, reflectivity, and mass of the satellite and R_{pm} is the distance from the sun to the satellite. Since the pressure force obeys the inverse square law, we may write $\bar{V} = \dfrac{\beta m}{R_{pm}}$ so that $F_\xi = -\ \dfrac{\partial V}{\partial \xi}$ is the pressure component in a given direction. This represents the radiation as coming from a point source.

---

[6] Also known as draconic period.

Its divergence is unrealistic in the case of solar radiation in terrestrial space and will be eliminated at a later point. In general the illumination of the satellite orbit will be nonuniform due to the Earth's shadow, albedo, and atmospheric absorption. We represent this nonuniformity as follows. Assume that the radiation source is fixed in space—then the orthogonal projection of the line *EP* on the orbital plane marks the constant angle $\bar{\theta}_0$ from the node (Fig. 6) and we introduce $\bar{\theta} = f + \theta_0 - \bar{\theta}_0 = f + \hat{\theta}_0$. Now the distribution of radiation intensity around the orbit will be approximated by the first two terms of a Fourier cosine series so that $\bar{V} = \dfrac{\beta m}{R_{pm}}(1 + b\cos\bar{\theta})$. With the usual simplifications we get

$$\bar{V}_u = \frac{\beta m r_c}{R_p{}^3}\Big[-1 - b\cos\bar{\theta} + \bar{x}\cos\theta + (\bar{y}\cos i + \bar{z}\sin i)\sin\theta$$
$$+ \tfrac{1}{2}b(\bar{y}\cos i + \bar{z}\sin i)[\sin(\theta + \bar{\theta}) + \sin(\theta_0 - \hat{\theta}_0)]$$
$$+ \tfrac{1}{2}b\bar{x}[\cos(\theta + \bar{\theta}) + \cos(\theta_0 - \hat{\theta}_0)]\Big],$$

$$\bar{V}_v = \frac{\beta m r_c}{R_p{}^3}\Big[[-\bar{x}\sin\theta + (\bar{y}\cos i + \bar{z}\sin i)\cos\theta$$
$$- \tfrac{1}{2}b\bar{x}[\sin(\theta + \bar{\theta}) + \sin(\theta_0 - \hat{\theta}_0)]$$
$$+ \tfrac{1}{2}b(\bar{y}\cos i + \bar{z}\sin i)[\cos(\theta + \bar{\theta}) + \cos(\theta_0 - \hat{\theta}_0)]\Big],$$

$$\bar{V}_w = \frac{\beta m r_c}{R_p{}^3}(\bar{z}\cos i - \bar{y}\sin i)(1 + b\cos\bar{\theta}),$$

where $\bar{x} = \dfrac{x_p}{r_c}$, $\bar{y} = \dfrac{y_p}{r_c}$, $\bar{z} = \dfrac{z_p}{r_c}$. Substitution of these expressions into Eqs. 20 to 22 yields

$$u = \bar{g}\Big[1 - \tfrac{1}{2}\bar{x}b\cos(\theta_0 - \hat{\theta}_0) - \tfrac{1}{2}(\bar{y}\cos i + \bar{z}\sin i)b\sin(\theta_0 - \hat{\theta}_0)$$
$$+ f[b\bar{x}\sin(\theta_0 - \hat{\theta}_0) - b(\bar{y}\cos i + \bar{z}\sin i)\cos(\theta_0 - \hat{\theta}_0)$$
$$+ \tfrac{1}{2}b\sin\bar{\theta} - \tfrac{3}{2}\bar{x}\sin\theta + \tfrac{3}{2}(\bar{y}\cos i + \bar{z}\sin i)\cos\theta]$$
$$+ \tfrac{1}{4}b\cos\bar{\theta} - \tfrac{7}{4}\bar{x}\cos\theta - \tfrac{7}{4}(\bar{y}\cos i + \bar{z}\sin i)\sin\theta$$
$$+ \tfrac{1}{3}b\bar{x}\cos(\theta + \bar{\theta}) + \tfrac{1}{3}b(\bar{y}\cos i + \bar{z}\sin i)\sin(\theta + \bar{\theta})\Big] \qquad (53)$$

$$\begin{aligned} v = \bar{g}\Big[&2b\bar{x}\sin(\theta_0 - \hat{\theta}_0) + b(\bar{y}\cos i + \bar{z}\sin i)\cos(\theta_0 - \hat{\theta}_0) \\ &+ f[\bar{x}(b\cos(\theta_0 - \bar{\theta}_0) - 3\cos\theta) + (\bar{y}\cos i + \bar{z}\sin i) \\ &\times \Big(b\sin(\theta_0 - \hat{\theta}_0) - 3\sin\theta\Big) - 2 + b\cos\bar{\theta}] \\ &+ f^2\tfrac{3}{4}b[(\bar{y}\cos i + \bar{z}\sin i)\cos(\theta_0 - \hat{\theta}_0) - \bar{x}\sin(\theta_0 - \hat{\theta}_0)] \\ &- \tfrac{3}{2}b\sin\bar{\theta} + \tfrac{11}{2}\bar{x}\sin\theta - \tfrac{11}{2}(\bar{y}\cos i + \bar{z}\sin i)\cos\theta \\ &\qquad - \tfrac{11}{24}b\bar{x}\sin(\theta + \bar{\theta}) + \tfrac{11}{24}b(\bar{y}\cos i + \bar{z}\sin i)\cos(\theta + \bar{\theta})\Big] \end{aligned} \tag{54}$$

$$w = \bar{g}(\bar{y}\sin i - \bar{z}\cos i)(1 + \tfrac{1}{4}b\cos\bar{\theta} + f\tfrac{1}{2}b\sin\bar{\theta}) \tag{55}$$

where $\bar{g} = \dfrac{\beta r_c{}^4}{GER_p{}^2}$.

We examine these results again for some special cases. If $x_p = y_p = 0$, $i = 0$, $b = 0$, $z_p = R_p$, the orbit lies in the x, y plane and is fully illuminated from the positive z-axis. Then $u = \bar{g}$, $v = -2f\bar{g}$, and $w = \bar{z}\bar{g}$. The meaning of w is obvious. It represents a slight translation of the orbit out of the x, y plane due to the uniform radiation pressure acting on it. From Fig. 7 it is clear that for m to be in equilibrium

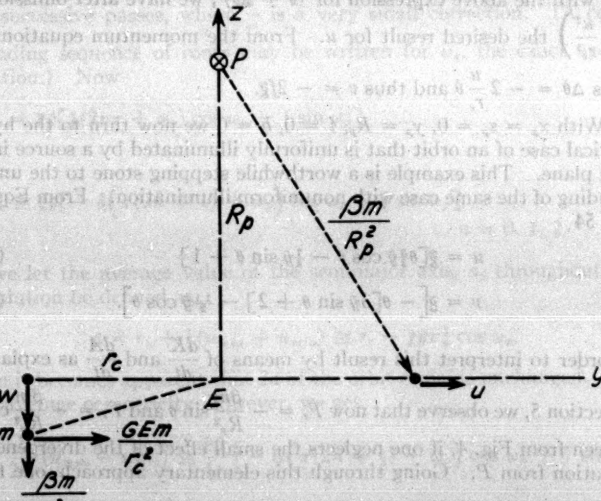

FIG. 7.

one requires $-\dfrac{w}{r_c} = \dfrac{\beta m}{R_p^2}\dfrac{r_c^2}{GEm}$ from which $w = -\dfrac{\beta r_c^3}{R_p^2 GE} = \bar{z}\tilde{g}$. The time-independent u component represents an enlargement of the orbit due to the radial pressure arising from the divergence of radiation from P and the linearly decreasing v is then necessary to conserve angular momentum. From the last condition

$$\dot{\theta} r_c^2 = (\dot{\theta} + \Delta\dot{\theta})(r_c + u)^2$$

and thus

$$(\dot{\theta} + \Delta\dot{\theta})^2 = \frac{GE}{r_c^3}\left(1 - 4\frac{u}{r_c} + O\left(\frac{u^2}{r_c^2}\right)\right).$$

From radial equilibrium

$$m(\dot{\theta} + \Delta\dot{\theta})^2(r_c + u) + \frac{\beta m r_c}{R_p^3} = \frac{GEm}{(r_c + u)^2}$$
$$= \frac{GEm}{r_c^2}\left(1 - 2\frac{u}{r_c} + O\left(\frac{u^2}{r_c^2}\right)\right),$$

and with the above expression for $(\dot{\theta} + \Delta\dot{\theta})^2$, we have after omission of $O\left(\dfrac{u^2}{r_c^2}\right)$ the desired result for u. From the momentum equation one finds $\Delta\dot{\theta} = -2\dfrac{u}{r_c}\dot{\theta}$ and thus $v = -2f\tilde{g}$.

With $x_p = z_p = 0$, $y_p = R_p$, $i = 0$, $b = 0$ we now turn to the hypothetical case of an orbit that is uniformly illuminated by a source in its own plane. This example is a worthwhile stepping stone to the understanding of the same case with nonuniform illumination. From Eqs. 53 and 54

$$u = \tilde{g}[\theta\tfrac{3}{2}\bar{y}\cos\theta - \tfrac{7}{4}\bar{y}\sin\theta + 1] \tag{53'}$$

$$v = \tilde{g}\Big[-\theta[3\bar{y}\sin\theta + 2] - \tfrac{11}{2}\bar{y}\cos\theta\Big]. \tag{54'}$$

In order to interpret this result by means of $\dfrac{dK}{dt}$ and $\dfrac{dA}{dt}$ as explained in Section 5, we observe that now $F_r = -\dfrac{\beta m}{R_p^2}\sin\theta$ and $F_t = -\dfrac{\beta m}{R_p^2}\cos\theta$, as seen from Fig. 4, if one neglects the small effect of the divergence of radiation from P. Going through this elementary approach, one finds

$$u = \tilde{g}\bar{y}[\theta\tfrac{3}{2}\cos\theta - \tfrac{7}{4}\sin\theta]$$

and

$$v = -\tilde{g}\bar{y}[\theta 3\sin\theta + \tfrac{11}{2}\cos\theta]$$

which differs from the exact expressions by the small terms $\tilde{g}$ and $-2\theta\tilde{g}$ and reflects the omission of the term $-\frac{\beta m r_c}{R_p{}^3}$ in V_u, as may be seen from substitution into Eq. 14. This discrepancy is, of course, due to the assumption of perfectly collimated light, which is true for solar radiation.

We observe that the amplitudes of u and v in this solution grow without bound as θ increases. One would indeed expect this result from the linearized equations for small oscillations about the circular path if the exciting forces F_r and F_t occur at resonance with the orbital frequency—which is the case. In terms of orbit shape this linearized model predicts ever-increasing eccentricity. Solving for the line of apsides, we have from $\frac{du}{d\theta} = 0$ that

$$\theta = -\tfrac{1}{6} \operatorname{ctn} \theta. \tag{56}$$

This results in the perigee locations

$$\omega_p = 3.08 + \frac{v(3.08)}{r_c}, \qquad 3.125 + \frac{v(2\pi + 3.125)}{r_c}, \cdots$$

for successive passes, where $\frac{v}{r_c}$ is a very small correction. (A corresponding sequence of roots may be written for ω_q, the exact apogee location.) Now

$$u_{\min} = \tilde{g}\bar{y}\left[\tfrac{3}{2}(2n\pi + \omega_p)\cos\omega_p - {}^{7}\sin\omega_p\right],$$

and (57)

$$u_{\max} \cong \tilde{g}\bar{y}\left[-\tfrac{3}{2}\Big(\pi(2n+1) + \omega_p\Big)\cos\omega_p + \tfrac{7}{4}\sin\omega_p\right],$$

$$n = 0, 1, 2 \cdots.$$

If we let the average value of the semimajor axis, a, throughout one revolution be defined as

$$\bar{a} = r_c + \tfrac{1}{2}(u_{\max} + u_{\min}) \cong r_c - \tilde{g}\bar{y}\pi\tfrac{3}{4}\cos\omega_p,$$

then it becomes apparent that $2a$ of the orbit remains unchanged. For the average eccentricity, however, we get

$$\bar{e} = \frac{1}{2r_c}(u_{\max} - u_{\min}) \cong \frac{\tilde{g}\bar{y}}{4r_c}\left[-6\Big(\pi(2n + \tfrac{1}{2}) + \omega_p\Big)\cos\omega_p + 7\sin\omega_p\right]$$

and

$$\frac{d\bar{e}}{d\theta} = \bar{e}' \cong -\frac{3\tilde{g}\bar{y}}{2r_c}\cos\omega_p.$$

For a 100-ft mylar balloon traveling in a 5000-mile orbit we find

$$\dot{\bar{e}} = \bar{e}'\dot{f} = -\frac{3\beta\cos\omega_p}{2R_p^2}\left(\frac{r_c}{GE}\right)^{1/2} = 1.65\ 10^{-7}/\text{sec.}$$

In a period of one month this would result in an eccentricity of 0.428 which is indeed prohibitive. Long before this condition is reached, other physical phenomena interact with the radiation pressure to shape the orbit. A more complete discussion of these perturbations will be given in Section 7.

If the orbit illumination is nonuniform, $b \neq 0$, then we have in place of Eq. 56

$$\theta = -\tfrac{1}{6}\operatorname{ctn}\theta + \tfrac{8}{9}b\cos\theta. \tag{56$'$}$$

With $b = 1$, this yields

$$\omega_p = 3.10 + \frac{v(3.10)}{r_c}, \qquad 3.126 + \frac{v(2\pi + 3.126)}{r_c}, \cdots.$$

In place of Eq. 57 we obtain

$$\left.\begin{aligned} &u_{\min} = \bar{g}\bar{y}\left[\tfrac{3}{2}(2n\pi + \omega_p)\cos\omega_p - \tfrac{7}{4}\sin\omega_p - b\left(\tfrac{1}{2} - \tfrac{1}{3}\cos 2\omega_p\right)\right] \\ &\text{and} \\ &u_{\max} \cong \bar{g}\bar{y}\left[-\tfrac{3}{2}\pi(2n+1)\cos\omega_p + \tfrac{7}{4}\sin\omega_p - b\left(\tfrac{1}{2} + \tfrac{1}{3}\cos\omega_p\right)\right] \\ &\hspace{18em} n = 0, 1, 2\cdots, \end{aligned}\right\} \tag{57$'$}$$

where the absence of a secular term in b happens to be due only to the fact that $\hat{\theta} = -\frac{\pi}{2}$. From this one can find estimates of $\bar{a}$ and $\bar{e}$ similar to the ones for $b = 0$ and subject to the same limitations.

We finally take $i \neq 0$ and maintain $x_p = z_p = 0$, $y_p = R_p$, $\theta_0 = 0$, and $b \neq 0$. Then

$$w = \bar{g}\bar{y}(1 + \tfrac{1}{4}b\sin\theta - \theta\tfrac{1}{2}b\cos\theta).$$

The secular term in this result again represents a precession and is due to the radiation moment M exerted on the orbit due to the term $b\cos\bar{\theta}$ of the intensity distribution. Using the arguments of Section 5, it can be shown that

$$M = \frac{b\beta m\sin i r_c}{2R_p^2}.$$

From this or from the expression for w one finds

$$\Delta w_{\min} = -\frac{\pi\beta r_c^3 b \sin i}{GER_p^2}. \tag{58}$$

If we take $\frac{\beta}{R_p^2} = 5.66\ 10^{-4}$ ft/sec² for the 100-ft mylar balloon, then $\dot{\Omega} = \frac{\beta b}{2R_p^2}\left(\frac{r_c}{GE}\right)^{1/2} = 1.228\ 10^{-8}$ rad/sec and $T_\Omega = 5850$ days for a 5000-mile orbit due to radiation pressure alone. The increment in the geo-period is $\Delta T_G = 0.095$ sec if $i = 20°$. One also observes that $\frac{di}{dt} = 0$, as in the case of Section 5.

As a last numerical result, we estimate Δi as produced on a 5000-mile polar orbit during one-eighth of a year when the sun travels in the x, y plane from the positive x-axis halfway to the positive y-axis (Fig. 6 with $i = 90°$, $\theta_0 = 0$). We note from Eq. 58 that the precession due to the radiation moment consists of a rotation $\dot{\varphi} = \frac{\Delta w_{\min}\dot{\theta}}{r_c 2\pi \cos i}$ about the line EP. Reinterpreting this result for the present situation we find $\frac{di}{dt} = \frac{\beta r_c^2 \sin \alpha\dot{\theta}}{2GER_p^2}$ where α is the angle from the positive x-axis to the sun. Thus,

$$\Delta i = \int_0^{\pi/4} \frac{\beta r_c^2\dot{\theta} \sin \alpha d\alpha}{2GER_p^2\sigma_s} = \frac{\beta r_c^2\dot{\theta}}{\sigma_s 2GER_p^2} 0.293 = 6.17\ 10^{-2} \text{ rad}$$

where σ_s is the angular rate of the sun in the geocentric frame. During the 2nd and 3rd octant of the sun's orbit the satellite is assumed uniformly illuminated and no precession takes place. In the 4th octant an equal and opposite effect to that of the 1st octant occurs. Thus the net effect of precession under radiation pressure vanishes in each half year.

7. COMBINED RESPONSE OF THE ORBIT TO RADIATION PRESSURE AND THE EQUATORIAL BULGE

In the preceding section we noted that the linearized equations of motion for a satellite on a nominal circular orbit give rise to unbounded u and v in response to radiation pressure within the orbital plane. At first sight one might expect the nonlinear equations of motion for this problem to impose a restriction on the magnitude of the response in the perturbations—in particular, one would hope for a bound on the eccentricity which keeps the perigee of the orbit at a sufficiently great altitude to avoid orbital collapse from atmospheric drag. In order to perform the nonlinear analysis, we now include terms to $O\left(\frac{u^3}{r_c^3}\right)$ in the expressions for the attraction by the central mass. Thus,

$$\left.\begin{aligned}\frac{\partial}{\partial u}\left(\frac{GEm}{r}\right) &= \frac{GEm}{r_c^2}\Big[1 - \frac{2u}{r_c} + 3\frac{u^2}{r_c^2} - \frac{3}{2r_c^2}(v^2 + w^2)\\ &\qquad + \frac{27}{2}\frac{u^3}{r_c^3} + \frac{6}{r_c^3}(uv^2 + uw^2) + O\left(\frac{u^4}{r_c^4}\right)\Big],\\ \frac{\partial}{\partial v}\left(\frac{GEm}{r}\right) &= \frac{GEm}{r_c^3}\Big[v - \frac{3}{r_c}uv + \frac{6}{r_c^2}u^2v\\ &\qquad - \frac{3}{2r_c^2}(v^3 + vw^2) + O\left(\frac{u^4}{r_c^4}\right)\Big]\\ \text{and}\qquad&\\ \frac{\partial}{\partial w}\left(\frac{GEm}{r}\right) &= \frac{GEm}{r_c^3}\Big[w - \frac{3}{r_c}uw + \frac{6}{r_c^2}u^2w\\ &\qquad - \frac{3}{2r_c^2}(v^2w + w^3) + O\left(\frac{u^4}{r_c^4}\right)\Big].\end{aligned}\right\} \quad (59)$$

If we substitute these expressions into Eqs. 5 to 7 together with $\tilde{V}_u = -\frac{\beta m}{R_p^2}\sin\theta$, $\tilde{V}_v = -\frac{\beta m}{R_p^2}\cos\theta$, and $\tilde{V}_w \equiv 0$ (since we have $i = 0$, $x_p = z_p = 0$, and $y_p = R_p$), then we may again eliminate p_u, p_v, p_w from Eqs. 5 to 10. We obtain

$$\begin{aligned}E_1 &= u'' - 2v' - 3u + b_1u^2 + b_2(v^2 + w^2)\\ &\qquad + b_3u^3 + b_4(uv^2 + uw^2) + V_1\sin\theta = 0 \quad (60)\\ E_2 &= v'' + 2u' - b_1uv + b_4u^2v + b_2(v^3 + vw^2) + V_1\cos\theta = 0\\ &\qquad w \equiv 0\end{aligned}$$

where

$$b_1 = \frac{3}{r_c}, \qquad b_2 = -\frac{3}{2r_c}, \qquad b_3 = \frac{27}{2r_c^2}, \qquad b_4 = \frac{6}{r_c^2},$$

$$V_1 = -\frac{\dot{\theta}^6\beta}{(GE)^4R_p^2},$$

and E_1 and E_2 shall be used as shorthand notation for the differential operators on u and v. By inspection of the linearized solution of Section 6, we may guess at the form $u = u_1\sin\theta + u_2\cos\theta$ and $v = v_1\sin\theta + v_2\cos\theta$. We now use this form to develop an approximate solution of Eq. 60 by the Ritz-Galerkin method. The Ritz conditions to be

V.2
196

satisfied are

$$\int_0^{2\pi} E_1 \sin\theta d\theta = 0, \qquad \int_0^{2\pi} E_1 \cos\theta d\theta = 0,$$

$$\int_0^{2\pi} E_2 \sin\theta d\theta = 0, \qquad \int_0^{2\pi} E_2 \cos\theta d\theta = 0.$$

Performing these quadratures, we obtain the four nonlinear algebraic equations in u_1, u_2, v_1, and v_2:

$$\left.\begin{aligned}
&4u_1 - 2v_2 - \tfrac{3}{4}(b_3u_1^3 + b_4u_1v_1^2) \\
&\qquad\qquad - \tfrac{1}{4}(3b_3u_1u_2^2 + b_4u_1v_2^2 + 2b_4u_2v_1v_2) = V_1 \\
&4u_2 + 2v_1 - \tfrac{1}{4}(3b_3u_1^2u_2 + 2b_4u_1\nu_1v_2 + b_4u_2v_1^2) \\
&\qquad\qquad - \tfrac{3}{4}(b_3u_2^3 + b_4u_2v_2^2) = 0 \\
&2u_2 + v_1 - \tfrac{3}{4}(b_4u_1^2v_1 + b_2v_1^3) \\
&\qquad\qquad - \tfrac{1}{4}\Big(b_4(u_2^2v_1 + 2u_1u_2v_2) + 3b_2v_1v_2^2\Big) = 0 \\
&-2u_1 + v_2 - \tfrac{1}{4}\Big(b_4(2u_1u_2v_1 + u_1^2v_2) + 3b_2v_1^2v_2\Big) \\
&\qquad\qquad - \tfrac{3}{4}(b_4u_2^2v_2 + b_2v_2^3) = V_1.
\end{aligned}\right\} \tag{61}$$

In the normal course of events one would now solve these nonlinear algebraic equations by a suitable numerical iteration scheme—and presumably a similar set of equations would be written and solved for $b \neq 0$. Unfortunately, however, the nonlinearities governed by the coefficients b_2 to b_4 in this problem turn out to be so feeble that the dynamic response of the satellite is very nearly described by the results of Section 6 if no additional phenomena enter the picture.

It turns out, however, that precession of the apsides due to the Earth's oblateness has a decisive influence on orbit distortion in this case. The reader will be aware of this shift in perigee from the literature. It is a nonuniform motion for inclined orbits but for equatorial orbits it simplifies to a steady rotation of the line of apsides, at the rate

$$\dot{\omega}_p = \frac{2\dot{f}Jr_E^2}{r_c^2} \tag{62}$$

where positive $\dot{\omega}_p$ is taken in the sense of the anomalistic motion $\jmath$. This precession occurs if an eccentric orbit, once it has been established, is left under the influence of the Earth's oblateness only.

Now let us recall the linearized effects of radiation pressure in a simplified form before we combine them with the perturbation from the equatorial bulge. We have learned that under the action of radiation pressure alone the secular term in u distorts the orbit according to $\tilde{u} = C\theta \cos\theta$ where perigee lies at $\theta \cong \pi$ and apogee at $\theta \cong 0$, $C = \frac{3}{2}\tilde{g}\bar{y}$, (and the symbol $\tilde{u}$ is used in distinction from u which will be reserved for the composite effect of oblateness and radiation pressure). This we have shown to be very nearly true after a small number of revolutions with the help of Eqs. 53′ and 56. Now it must also be pointed out that the orbit distortion as given by $\tilde{u}$ does not exhibit the exact form of a cosine function for any one complete revolution. This is due to the time-dependent amplitude term in $\tilde{u}$. The cosine shape describes an osculating locus only which the satellite would follow if at any one instant the perturbing radiation were eliminated.[7] If however we assume that $C \ll 1$, then the individual pass of the satellite very closely approximates a cosinusoidal departure which is superimposed on the nominal circular shape but whose amplitude changes appreciably only over a large number of revolutions. This assumption is a convenient one and a reasonable one to make in the present case.

Now we proceed to combine what we have learned about the individual actions of the equatorial bulge and the radiation pressure to obtain the following picture. During each revolution of the satellite a distortion $\tilde{u}_n = CfT_A \cos f$ is impressed on the orbit by the radiation pressure; but in the same time all such terms that were previously generated have shifted along the orbit by the phase angle $\Delta\gamma = \dot{\omega}_p T_A$, where T_A is the anomalistic period. The composite perturbation of the orbit is then

$$F(\theta, N_1) = \sum_{n=0}^{N_1} CfT_A \cos(\theta - n\Delta\gamma) \tag{63}$$

up to N_1 revolutions of the satellite. In writing this expression we have not only applied linear superposition to the perturbations from oblateness and radiation pressure but also to the effects of individual revolutions. Substituting $T_A = \dfrac{\Delta\gamma}{\dot{\omega}_p}$ and $c = \dfrac{Cf}{\dot{\omega}_p}$ and letting $\Delta\gamma \to 0$, $N_1 \to \infty$ such that $N_1\Delta\gamma = \gamma_1$ we have

$$\begin{aligned} F(\theta, \gamma_1) &= \lim_{\Delta\gamma\to 0} \sum_{n=0}^{N_1} c\Delta\gamma \cos(f - n\Delta\gamma) \\ &= c\int^{\gamma_1} \cos(f - \gamma)d\gamma = c[\sin\theta - \sin(\theta - \gamma_1)] \\ &= 2c \sin\frac{\gamma_1}{2} \cos\left(\theta - \frac{\gamma_1}{2}\right). \end{aligned}$$

---

[7] Another way of visualizing the osculating orbit may be obtained by the [illegible] ken-experiment": Imagine that the satellite is dissolved into a string of pa[illegible] continuously distributed around the orbit (for example, an artificial ionosphere). T[illegible] barring all complementary solutions by a suitable choice of initial conditions for each particle, this ring of distributed mass will indeed exhibit a cosine distortion at every instant whose amplitude however is time-dependent according to $\tilde{u}$.

We see now that the resultant orbital distortion is again a cosine function in θ which, however, proceeds around the orbit at an angular rate which is half the precession due to oblateness. Thus, the apsidal motion of the resultant orbit is $f_p = \frac{1}{2}\dot{\omega}_p$. Since the amplitude of the perturbation varies periodically in $\frac{\gamma_1}{2}$, we note in particular that $F_{\min} = -2c \sin\frac{\gamma_1}{2}$. Thus, perigee first originates at $f_p = \pi$, then shifts to $f_p = \frac{3\pi}{2}$ where it attains a maximum amplitude of $-2c$, proceeds to $f_p = 2\pi$ where it vanishes, and immediately reappears at $f_p = \pi$ since what used to be apogee now turns into perigee with the change of sign in $\sin\frac{\gamma_1}{2}$ of Eq. 64.[8]

One notes that no changes need be made in the above analysis if the line *EP* were to rotate with respect to an inertial reference frame at the rate σ_s. We merely change the notation from θ to θ_r and replace $\dot{\omega}_p$ by $\dot{\omega}_{pr} = \dot{\omega}_p - \sigma_s$, to indicate that these quantities are measured in the rotating frame.

If we take the maximum perigee depression as a measure of orbit feasibility, we have

$$2c = \frac{3\bar{g}\bar{y}\dot{f}}{(\dot{\omega}_p - \sigma_s)} = \frac{3\beta r_c^3}{GER_p^2}\Big/\left[2\frac{Jr_E^2}{r_c^2} - \sigma_s\left(\frac{r_c^3}{GE}\right)^{1/2}\right]. \tag{65}$$

For a 5000-mile orbit this amounts to 115 mi. and for a 26,250-mile orbit to 11,400 mi. We also have for the 5000-mile orbit: $\dot{\omega}_{pr} = 1.6\ 10^{-6}$ rad/sec; duration of one sweep of perigee = 45 days; and range of one sweep of perigee = 3.91 rad (in an inertial frame). For the 24-hr orbit: $\dot{\omega}_{pr} = -1.93\ 10^{-7}$ rad/sec; duration = 377 days; and range = 3.33 radians.

8. SUMMARY AND CONCLUSIONS

Reviewing the material in Sections 3 to 7, we note that Hamilton's canonical equations lend themselves remarkably well to the solution of satellite perturbation problems in terms of position coordinates *versus* time. Orbit sensitivities to errors of injection and observation as well as the perturbations from various geophysical effects may be calculated. We recall in particular the following numerical results from the analyses of circular orbits.

If we wish to establish an orbit whose shape after discounting perturbations due to the equatorial bulge is a circle of 5000-mile radius at an inclination of $i = 51°$, with the cut-off point at $\theta_0 = 50°$

---

[8] It is also seen that Eq. 64 gives the shape of an artificial ionosphere as a function of γ_1, that is, time. This does not include "tidal effects."

from the node and at a cut-off radius of 5000 miles, then the necessary change of injection velocity from the circular value is $\Delta V = -4.37$ ft/sec and the correction in azimuth $\Delta\psi = -\frac{\dot{\bar{w}}_0}{r_c} = -0.33\ 10^{-3}$ rad. In spite of these corrections the angular motion will show the discrepancy $\Delta\dot{\theta} = 4.23\ 10^{-8}$ rad/sec. If we insist on a mean velocity and launch velocity equal to the circular value, we need to cut off at an increase of altitude $\bar{u}_0 = 245$ ft and the resultant mean radius will be increased by $\Delta r_c = 858$ ft. The maximum amplitude of the periodic perturbations which are impressed on the circle amounts to about 7000 ft.

The periodic perturbations on a 24-hr satellite in the equatorial plane by the moon's gravitation will amount to about 3000 ft in the circumferential direction which, indeed, is negligible for practical purposes. However, a guidance tolerance of ±1 ft/sec in the injection velocity or subsequent corrections of circumferential velocity to that accuracy will ensure an operating period of only 93 days before the satellite drifts out of an allowable geocentric sight-angle of ±10°. If a 24-hr satellite were put into orbit at an inclination of 20°, the regression of the nodes due to the moon and sun combined would amount to $\dot{\Omega} = -1.12\ 10^{-9}$ rad/sec. This reduces the nodal period of 27,956 days, which is due to oblateness alone, by 8418 days. The decrement of the geo-period amounts to -1.24 sec.

Solar radiation pressure acting alone on a 100-ft mylar balloon of 0.0005-in. thickness produces the following perturbations. If the orthogonal projection of the line *ES* on the orbit plane marks the angle $\bar{\theta}_0$ from the node in the direction of satellite motion then a perigee will be impressed on the initially circular orbit at approximately $\bar{\theta}_0 + \frac{\pi}{2}$. This location of the apsides is quite insensitive to the intensity distribution of the incident radiation around the orbit. Furthermore, no appreciable change occurs in the semimajor axis of the orbit. The rate at which eccentricity is being accumulated, however, is of the order $1.65\ 10^{-7}$/sec for a 5000-mile orbit. According to this analysis the satellite would scarcely have a lifetime of a month. If, however, the precession of apsides due to the equatorial bulge is included, then the following perturbations result. A 5000-mile orbit in the equatorial plane will develop a periodic perigee with a maximum depression of $u_{\min} = -115$ mi. and a precessional rate of $\dot{f}_p = 10^{-6}$ rad/sec in an inertial frame. The duration of one sweep in perigee between zero amplitudes is $T_p = 45$ days and the angular range through which the perigee travels in each sweep relative to an inertial frame is $\Delta\theta = 3.913$ rad. The corresponding quantities for a 24-hr satellite are: $u_{\min} = -11{,}400$ mi.; $\dot{f}_p = 1.03\ 10^{-7}$ rad/sec; $T_p = 377$ days; and $\Delta\theta = 3.33$

rad. If a mylar balloon were put into a 5000-mile polar orbit, then the moment exerted by radiation pressure on this orbit may perturb the inclination by as much as $6.2\ 10^{-2}$ rad in one and a half months—the net effect over each half-year, however, reduces to zero. If the same orbit is inclined at $i = 20°$, we obtain a nodal precession rate of the order $1.228\ 10^{-8}$ rad/sec which turns out to be $\frac{1}{17}$ in magnitude of the regression due to the equatorial bulge for an orbit of this size. The increment in the geo-period amounts to 0.095 sec.

Some order-of-magnitude checks of the above results have been obtained by a digital simulation. Work in this direction continues and will be reported at a later time.

A FURTHER CREEP ANALYSIS FOR ROTATING SOLID DISKS OF VARIABLE THICKNESS

BY

B. M. MA[1]

ABSTRACT

A further creep analysis for stress distributions in rotating solid disks of variable thickness and at uniform temperature is presented herein, based on the Tresca criterion and its associated flow rule. The advantage of this analysis lies in the fact that the complicated problem is to be solved in great simplicity.

Disks of gas turbines and jet engines are usually operated at relatively high stresses and high temperatures. Therefore, in this paper the stress analysis for the variable-thickness and uniform-temperature disk at steady-state conditions will be analyzed and discussed by using the exponential function stress-creep-rate relation.

Illustrative examples for computing the stress distributions of the variable-thickness and uniform-temperature disk will be presented on the basis of theoretical analysis. For the purpose of comparison the stress distributions for the constant-thickness and uniform-temperature disk will also be given. It will be found that the stress distributions over certain central portions of the disk are quite different between the variable- and constant-thickness disks.

NOMENCLATURE

The following nomenclature is used in the paper:

a = constant
c, m = constants
$h = f(r) = cr^m = cr_o^m x^m$ = thickness of disk
k, K = constants
n = material creep number
r = radius to any point of disk
r_i = inner radius of disk
r_o = outer radius of disk
r_e = radius to the point x_e of disk
t = time
T = absolute temperature
$\dot{u}$ = rate of radial displacement of disk at radius r
$x = r/r_o$
$x_i = r_i/r_o$
$x_e = r_e/r_o$
σ = equivalent or effective stress
$\sigma_a = \rho\omega^2 r_o^2$ = equivalently inertial stress in rotating thin ring of radius r_o
σ_0 = material creep modulus, having dimensions of stress
$\sigma_1, \sigma_2, \sigma_3$ = principal stresses along axes 1, 2 and 3, respectively
$\sigma_t, \sigma_r, \sigma_z$ = tangential, radial and axial stresses of disk, respectively
σ_{r_o} = radial stress at r_o of disk
σ_{r_e} = radial stress at x_e
σ_{t_e} = tangential stress at x_e
$\dot{\epsilon}$ = creep rate or effective creep rate

---

[1] Department of Mechanical Engineering, South Dakota State College, Brookings, S. D.

$\dot{\epsilon}_1, \dot{\epsilon}_2, \dot{\epsilon}_3$ = principal creep rates along axes 1, 2 and 3, respectively
$\dot{\epsilon}_t, \dot{\epsilon}_r, \dot{\epsilon}_z$ = tangential, radial and axial creep rates of disk, respectively
$\epsilon_1, \epsilon_2, \epsilon_3$ = principal creep strains along axes 1, 2 and 3, respectively
$\rho = \gamma/g$ = density of disk material
γ = specific weight of disk material
g = gravitational acceleration
ω = angular speed of disk

1. INTRODUCTION

In a previous paper (**1**),[2] some formulas were derived for calculating creep deformations and stress distributions in rotating solid disks of variable thickness and uniform temperature. These formulas were based on the maximum shear theory associated with the Mises flow rule, and also under the restriction that the tangential stresses are invariably greater than the radial stresses in the disk, except at the center of the disk. The results obtained appear to be relatively simple, reasonable and in excellent agreement with the creep test data (**2**) when compared with the results found using the distortion energy theory.

This paper, however, is based on the theory of the Tresca Criterion and its associated flow rule. The restriction on the stresses $\sigma_t > \sigma_r$ over the whole disk is also removed. In general, the stress distributions in the disk are divided into the two regions below:

$$\begin{array}{lll} 1.\ \sigma_t > \sigma_r > 0 & \text{for} & x_e \leq x \leq 1 \\ 2.\ \sigma_t = \sigma_r > 0 & \text{for} & x_i \leq x \leq x_e \end{array}$$

and the stress equations are obtained in the closed form without resorting to the successive approximation method.

Stress distributions in region 2 of the disk can be analyzed by recognizing the fact that radial stresses are frequently equal to tangential stresses near the center and over a portion of the disk (**3**). This is true because the centrifugal loading or inertial forces of turbine blades are transmitted through the rim of the disk to the disk proper, that is, the radial stress σ_{r_0}, acting on the outer radius of the disk. The greater the value of σ_{r_0} is, the more the stress condition, $\sigma_t = \sigma_r$, of region 2 over a portion of the disk spreads toward r_0.

Experimental data also show that the yield and bursting speeds of hollow disks are materially reduced by the presence of a bore, because the presence of this bore is equivalent to introducing a stress concentration factor at this point of the disks. The reduction of these yield and bursting speeds is generally in proportion to the section area of material removed (**4**). For this reason, in many practical applications of high-speed gas turbines and jet engines, solid disks without bores are adopted when the disks are made integral with the shaft. Of course, the magnitude of σ_{r_0}, which is directly proportional to the square of the speed, is also increased with the increasing speeds.

---

[2] The boldface numbers in parentheses refer to the references appended to this paper.

Based on the Tresca criterion and its associated flow rule, and using the power function stress-creep-rate relation, the constant thickness solid disk at the steady-state condition has been treated by Wahl (5). In the present paper, on the basis of the same criterion and flow rule, we use the exponential function stress-creep-rate relation at steady-state condition. The variable-thickness solid disk will be analyzed and discussed. Examples applying to the theoretical analysis for stress distributions of the disk will also be given.

2. CREEP RATE AND STRAIN EQUATIONS

In general, for a given material, creep rate is primarily a function of stress, time and temperature, as given in the previous paper (1). Now, on this basis it follows that creep rate $\dot{\epsilon}$ is equal to the product of a function of stress, $F(\sigma)$, a function of time, $f(t)$, and a function of temperature $g(T)$, or

$$\epsilon = F(\sigma)f(t)g(T). \tag{1}$$

It is further assumed that the function of stress, $F(\sigma)$, may be represented by

(*a*) the power function creep law, σ^n, for relatively low stresses or low temperatures,
(*b*) the exponential function creep law, e^{σ/σ_0}, for relatively high stresses or high temperatures,

where σ is the equivalent or effective stress, n the "material creep number," and σ_0 the "material creep modulus."

Based on the basic assumptions given in the previous paper (1), and that the yield condition obeys the Tresca criterion and its associated flow rule, Eq. 1 may be written as follows:

$$\left.\begin{aligned} &\epsilon_1 = -\dot{\epsilon}_3 = k\sigma^n e^{-a/T} f(t), \quad \text{for} \quad \sigma_1 > \sigma_2 > \sigma_3 \\ &\dot{\epsilon}_2 = 0 \end{aligned}\right\} \tag{2a}$$

$$\left.\begin{aligned} &\dot{\epsilon}_1 = \lambda k\sigma^n e^{-a/T} f(t) \\ &\dot{\epsilon}_2 = (1-\lambda)k\sigma^n e^{-a/T} f(t) \quad \text{for} \quad \sigma_1 = \sigma_2 > \sigma_3 \quad \text{and} \quad 0 \leq \lambda \leq 1 \\ &\dot{\epsilon}_3 = -k\sigma^n e^{-a/T} f(t) \end{aligned}\right\} \tag{2b}$$

for the power function stress-creep-rate relation, and

$$\epsilon_1 = -\dot{\epsilon}_3 = Ke^{\sigma/\sigma_0} e^{-a/T} f(t), \quad \dot{\epsilon}_2 = 0 \quad \text{for} \quad \sigma_1 > \sigma_2 > \sigma_3 \tag{3a}$$

$$\left.\begin{aligned} &\dot{\epsilon}_1 = \lambda Ke^{\sigma/\sigma_0} e^{-a/T} f(t) \\ &\dot{\epsilon}_2 = (1-\lambda)Ke^{\sigma/\sigma_0} e^{-a/T} f(t) \quad \text{for} \quad \sigma_1 = \sigma_2 > \sigma_3 \quad \text{and} \quad 0 \leq \lambda \leq 1 \\ &\dot{\epsilon}_3 = -Ke^{\sigma/\sigma_0} e^{-a/T} f(t) \end{aligned}\right\} \tag{3b}$$

for the exponential function stress-creep-rate relation, where λ is a multiplier or a parameter which will be further defined later, and the constants k and K may be determined from creep test data. Upon integration of Eqs. 2 and 3, the creep strains are, respectively, obtained.

$$\epsilon_1 = -\epsilon_3 = k\sigma^n \int_0^t e^{-a/T} f(t)dt, \quad \epsilon_2 = 0 \quad \text{for} \quad \sigma_1 > \sigma_2 > \sigma_3 \qquad (4a)$$

$$\epsilon_1 = \lambda k\sigma^n \int_0^t e^{-a/T} f(t)dt, \text{ etc.} \qquad \text{for} \quad \sigma_1 = \sigma_2 > \sigma_3 \qquad (4b)$$

and

$$\epsilon_1 = -\epsilon_3 = Ke^{\sigma/\sigma_0} \int_0^t e^{-a/T} f(t)dt, \quad \epsilon_2 = 0 \quad \text{for} \quad \sigma_1 > \sigma_2 > \sigma_3 \qquad (5a)$$

$$\epsilon_1 = \lambda Ke^{\sigma/\sigma_0} \int_0^t e^{-a/T} f(t)dt, \text{ etc.}$$
$$\text{for} \quad \sigma_1 = \sigma_2 > \sigma_3 \quad \text{and} \quad 0 \leq \lambda \leq 1 \qquad (5b)$$

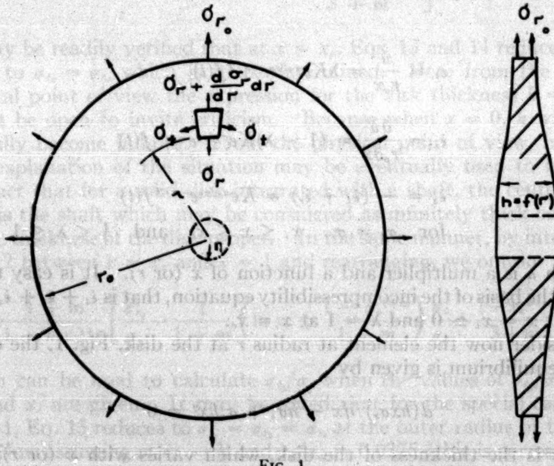

FIG. 1.

in which the initial creep strains are assumed to be zero at $t = 0$. Remember that for the steady-state condition, the stresses are independent of the time, while the temperature and the time may depend upon each other.

As mentioned before, turbine disks of jet propulsion units are usually operated under the condition of relatively high stresses and high temperatures. For this reason in the present paper, we shall limit further discussion to the exponential function stress-creep-rate relation only.

3. CREEP ANALYSIS IN ROTATING DISK WITH VARIABLE THICKNESS AND UNIFORM TEMPERATURE—STEADY-STATE CONDITION

On the basis of the basic assumptions given in the previous paper (1) the principal stresses in the disk, Fig. 1, may take the following biaxial stress system:

$$\sigma_t \geq \sigma_r > \sigma_z = 0, \quad \sigma_t = \sigma \quad \text{for} \quad \sigma_t \equiv \sigma_1, \quad \sigma_r \equiv \sigma_2, \quad \sigma_z \equiv \sigma_3. \tag{6}$$

Now, substituting this sytem into Eq. 3, we may have (1)

$$\dot{\epsilon}_t = -\dot{\epsilon}_z = \frac{\dot{u}}{r_o x} = K e^{\sigma_t/\sigma_0} e^{-a/T} f(t) \tag{7}$$

$$\dot{\epsilon}_r = \frac{\partial \dot{u}}{r_o \partial x} = 0 \quad \text{for} \quad \sigma_t > \sigma_r \quad \text{and} \quad x_c \leq x \leq 1; \tag{8}$$

and

$$\epsilon_t = \frac{\dot{u}}{r_o x} = \lambda K e^{\sigma_t/\sigma_0} e^{-a/T} f(t) \tag{9}$$

$$\dot{\epsilon}_r = \frac{\partial \dot{u}}{r_o \partial x} = (1 - \lambda) K e^{\sigma_t/\sigma_0} e^{-a/T} f(t) \tag{10}$$

$$\dot{\epsilon}_z = -(\dot{\epsilon}_t + \dot{\epsilon}_r) = K e^{\sigma_t/\sigma_0} e^{-a/T} f(t)$$
$$\text{for} \quad \sigma_t = \sigma_r, \quad x_i \leq x \leq x_c \quad \text{and} \quad \tfrac{1}{2} < \lambda \leq 1 \tag{11}$$

in which λ is a multiplier and a function of x (or r). It is easy to see that on the basis of the incompressibility equation, that is $\dot{\epsilon}_t + \dot{\epsilon}_r + \dot{\epsilon}_z = 0$, $\lambda \simeq \frac{1}{2}$ at $x = x_i \simeq 0$ and $\lambda = 1$ at $x = x_c$.

Consider now the element at radius r at the disk, Fig. 1, the equation of equilibrium is given by

$$d(hx\sigma_r)/dx - h\sigma_t + \sigma_a h x^2 = 0 \tag{12}$$

where h is the thickness of the disk, which varies with x (or r), and $\sigma_a = \rho\omega^2 r_o^2$, the equivalent inertial stress in rotating thin ring of radius r_o.

Outer Region of the Disk $\sigma_t > \sigma_r > 0$, $x_c \leq x \leq 1$

Differentiating Eq. 7 with respect to x, in which substituting from Eqs. 7 and 8, respectively, for $\dot{u}/r_o x$ and $\partial \dot{u}/r_o \partial x$, it follows that $1/x$

$= -d\sigma_t/\sigma_0 dx$. Integrating this between x_c and x, we have the non-dimensional form for the tangential stress

$$\sigma_t/\sigma_a = \sigma_{t_c}/\sigma_a - \sigma_0/\sigma_a \ln \frac{x}{x_c} \tag{13}$$

in which σ_{t_c} is the value of σ_t at $x = x_c$. Now, consider the hyperbolic profile of the disk with the form $h = cr_o{}^m x^m$ (where c and m are constant, but m is a negative value). By substituting this thickness function and Eq. 13 into Eq. 12 and integrating between x_c and x, we have for the radial stress

$$\begin{aligned}\frac{\sigma_r}{\sigma_a} = \frac{1}{x^{1+m}}\Bigg[& \frac{x^{1+m} + mx_c{}^{1+m}}{1+m}\,\frac{\sigma_{t_c}}{\sigma_a} \\ & - \frac{1}{1+m}\left(x^{1+m} \ln \frac{x}{x_c} - \frac{x^{1+m} - x_c{}^{1+m}}{1+m}\right) \\ & - \frac{x^{3+m} - x_c{}^{3+m}}{3+m}\Bigg] \quad x_c \leq x \leq 1.\end{aligned} \tag{14}$$

It may be readily verified that at $x = x_c$, Eqs. 13 and 14 reduce identically to $\sigma_{t_c} = \sigma_{r_c}$ which is to be determined. Here from the mathematical point of view the expression for the disk thickness $h = cr_o{}^m x^m$ might be open to invite criticism. Because when $x = 0$, h will theoretically become infinite. From the physical point of view, however, this explanation of the situation may be eventually used to interpret the fact that for a solid disk integrated with a shaft, the center of the disk is the shaft which may be considered as infinitely thick compared to the thickness of the disk proper. In the same manner, by integrating Eq. 12 between $x = x_c$ and $x = 1$ and rearranging, we obtain

$$\frac{\sigma_{t_c}}{\sigma_a} = \frac{1+m}{1+mx_c{}^{1+m}}\left[\frac{\sigma_{r_c}}{\sigma_a} - \frac{1}{1+m}\left(\ln x_c + \frac{1 - x_c{}^{1+m}}{1+m}\right)\frac{\sigma_0}{\sigma_a} + \frac{1 - x_c{}^{3+m}}{3+m}\right] \tag{15}$$

which can be used to calculate σ_{t_c}/σ_a when the values of σ_{r_c}/σ_a, σ_o/σ_a, m, and x_c are given. It may be noted that for the special case when $x_c = 1$, Eq. 15 reduces to $\sigma_{t_c} = \sigma_{r_c} = \sigma_{r_o}$ at the outer radius of the disk, r_o. Now assuming $m = -\frac{1}{2}$, and $\sigma_0/\sigma_a = 0.0275$ (this is corresponding to the assumption that $\sigma_0 = 7{,}000$ psi, and $\sigma_a = 254{,}000$ psi at the speed of the disk 17,800 rpm and the specific weight of the material $\gamma = 0.284$ lb per cu. in.), the values of σ_{t_c}/σ_a *versus* x_c are plotted for various values of σ_{r_c}/σ_a, Fig. 2.

It is seen that in this figure the peaks of σ_{t_c}/σ_a *versus* x_c shift to the right or outward from the center of the disk as the values of σ_{r_c}/σ_a increase. It may be mentioned here that for $m = -\frac{1}{2}$ and $r = 10$, the thickness distribution of the disk profile is similar to that shown in Fig. 1.

To determine the value of the critical point x_c for which the condition, $\sigma_t = \sigma_r > 0$, is fulfilled and thereby Eqs. 13 and 14 will not hold anymore. Now, we divide Eq. 14 by Eq. 13, differentiate this ratio σ_r/σ_t with respect to x and set it equal to zero for a maximum at $x = x_c$. It yields

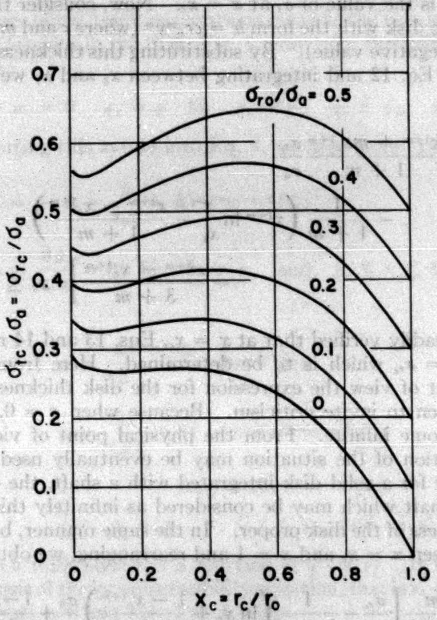

FIG. 2. Tangential stresses at x_c for various values of σ_{ro}/σ_a, $m = -\frac{1}{2}$, $\sigma_o/\sigma_a = 0.0275$.

$$\frac{\sigma_{t_c}}{\sigma_a} - \frac{1}{m}\left(\frac{\sigma_0}{\sigma_a} - x_c^2\right) = 0 \tag{16}$$

with given values of σ_{t_c}/σ_a, σ_0/σ_a, r_o and m, x_c can be readily found. For example, let $\sigma_{t_c}/\sigma_a = 0.176$, $\sigma_0/\sigma_a = 0.0275$, and $m = -\frac{1}{2}$; the critical value of x_c is approximately equal to 0.340. In this particular case, any value of x_c less than 0.340 will not meet the required condition, $\sigma_t > \sigma_r > 0$, over a portion of the outer region of the disk.

7.269
1960

Inner Region of the Disk $\sigma_t = \sigma_r > 0,\ x_i \le x \le x_c,\ \frac{1}{2} < \lambda \le 1$

In this region of the disk, since $\sigma_t = \sigma_r$ for $x_i \le x \le x_c$, Eq. 12 may be integrated between x and x_c. Upon substitution of $h = cr_o{}^m x^m$ and integration, we have

$$\frac{\sigma_t}{\sigma_a} = \frac{\sigma_r}{\sigma_a} = \left(\frac{x_c}{x}\right)^m \frac{\sigma_{t_c}}{\sigma_a} + \frac{x_c{}^{2+m} - x^{2+m}}{(2+m)x^m} \quad x_i \le x \le x_c. \tag{17}$$

In order to determine the value of λ if it satisfies the condition $\frac{1}{2} < \lambda \le 1$ for $x_i \le x \le x_c$, at first, we differentiate Eq. 9 with respect to x, (remember that λ is a function of x), next, we use Eqs. 9 and 10 for substituting $\dot{u}/r_o x$ and $\partial\dot{u}/r_o\partial x$ as before and finally we rearrange, getting

$$d\lambda/dx = (2/x + d\sigma_t/\sigma_0 dx) = 1/x.$$

Integrating this between x and x_c and taking $\lambda = 1$ at $x = x_c$, we have

$$\lambda = \left(\frac{x_c}{x}\right)^2 e^{(\sigma_{t_c} - \sigma_t)/\sigma_0} + \frac{1}{x^2 e^{\sigma_t/\sigma_0}} \int_x^{x_c} x e^{\sigma_t/\sigma_0} dx \quad x_i \le x \le x_c \tag{18}$$

in which σ_{t_c} is given by Eq. 15 and σ_t is given by Eq. 17. By substituting the value of σ_t from Eq. 17 into the integrand of Eq. 18 and

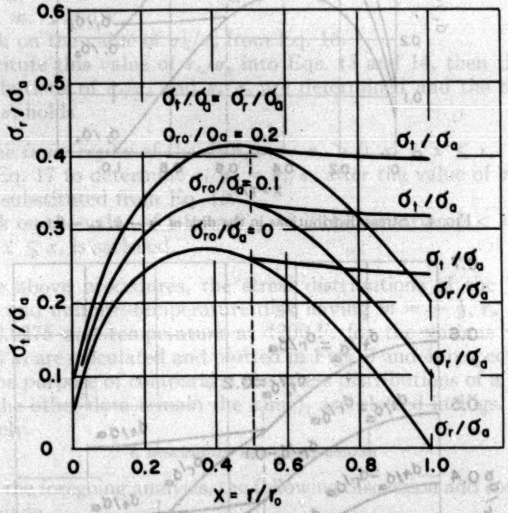

FIG. 3. Stress distribution in the disk $m = -\frac{1}{2}$, $x_c = 0.5$.

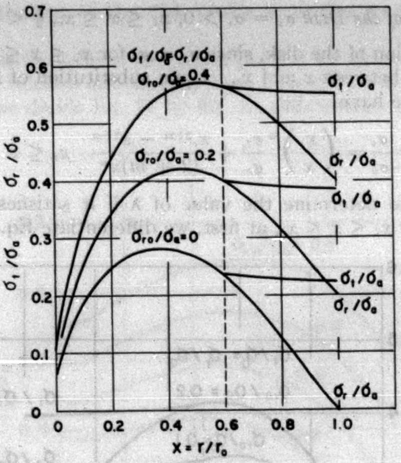

FIG. 4. Stress distributions in the disk $m = -\frac{1}{2}$, $x_e = 0.6$.

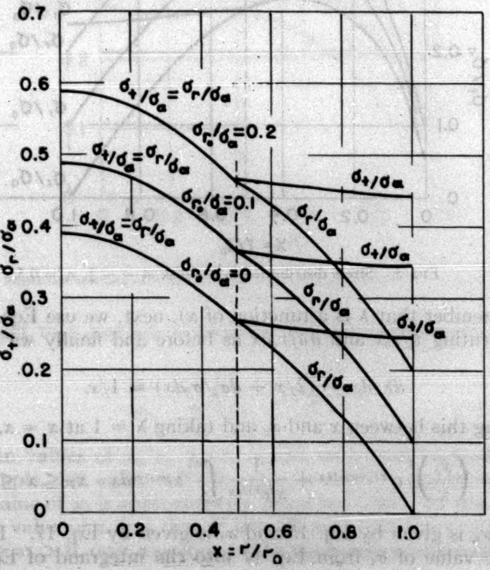

FIG. 5. Stress distribution in flat disk $m = 0$, $x_e = 0.5$.

introducing a new variable the integration for λ for given value of m may be found. Experience shows, however, that by a numerical evaluation of the integral in Eq. 18 it is relatively simple to determine whether the condition $\frac{1}{2} < \lambda \leq 1$ holds for $x_i \leq x \leq x_e$ or not; a check reveals that this is usually true.

The procedures for the creep analysis of variable-thickness and uniform-temperature disk in the present paper may be summed up as follows.

For the *outer region* of the disk, $\sigma_t > \sigma_r > 0$ for $x_e \leq x \leq 1$:

(*a*) Use Eq. 15 to determine σ_{t_e}/σ_a for prescribed values of σ_{r_o}/σ_a, σ_0/σ_a, m, r_o and x_c.
(*b*) Check on the value of σ_{t_e}/σ_a from Eq. 16.
(*c*) Substitute this value of σ_{t_e}/σ_a into Eqs. 13 and 14, then the stress distributions of σ_t/σ_a and σ_r/σ_a are determined and the condition $\sigma_t > \sigma_r$ holds.

For the *inner region* of the disk, $\sigma_t = \sigma_r > 0$, $x_i \leq x \leq x_e$:

(*d*) Use Eq. 17 to determine $\sigma_t/\sigma_a = \sigma_r/\sigma_a$ after the value of σ_{t_e}/σ_a has been substituted from Eq. 15.
(*e*) Check on the value of λ from Eq. 18 if the condition $\frac{1}{2} < \lambda \leq 1$ for $x_i \leq x \leq x_e$ is satisfied.

From the above procedures, the stress distributions of the variable-thickness and uniform-temperature disk having $m = -\frac{1}{2}$, $r_o = 10$ in., $\sigma_0/\sigma_a = 0.0275$ and temperature at 1200 F. for the various values of σ_{r_o}/σ_a and x_e are calculated and plotted in Figs. 3 and 4, respectively.

For the purpose of comparison the stress distributions of a flat disk, $m = 0$ (the other data remain the same), are plotted in Figs. 5 and 6, respectively.

4. DISCUSSION AND CONCLUSIONS

From the foregoing analysis, the following discussion and conclusions may be made.

1. Based on the Tresca criterion, from Eq. 3*a* the effective creep rate $\dot{\epsilon}$ corresponding to the effective stress σ is given by

$$= 2Ke^{\sigma/\sigma_0}e^{-a/T}f(t). \tag{19}$$

At the steady-state condition and the given temperature, the stresses will be independent of time and temperature. Then, by differentiating Eq. 19 with respect to σ, the slope of the creep curves for the exponential function stress-creep-rate relation is obtained.

$$d\dot{\epsilon}/d\sigma = \dot{\epsilon}/\sigma_0. \tag{20}$$

It is seen that for a given material, by using Eq. 20, the value of creep material modulus σ_0 may be readily determined from simple tension creep-test data. In the previous example the value of σ_0 is taken approximately for the disk material of Cr-Ni alloy steel at 1200 F. (6).

2. From Figs. 3 and 4 for the variable-thickness disk of $m = -\frac{1}{2}$, it is seen that the peak stresses in the disk increase with the values of σ_{r_o}/σ_a and x_c and have a tendency to shift toward the outer radius r_o.

3. Equations 14, 15, 16 and 17 for the variable-thickness disks can be immediately reduced to that for the flat disk when $m = 0$, Eqs. 13 and 18 remain in the same form, but the numerical value of σ_t/σ_a changes with that of σ_{t_e}/σ_a according to the changes of Eqs. 15 and 17, respectively. The maximum stresses in the flat disk, Figs. 5 and 6, occurred at the center of the disk are as anticipated. They are quite, however, contrary to that of the variable-thickness disk, Figs. 3 and 4.

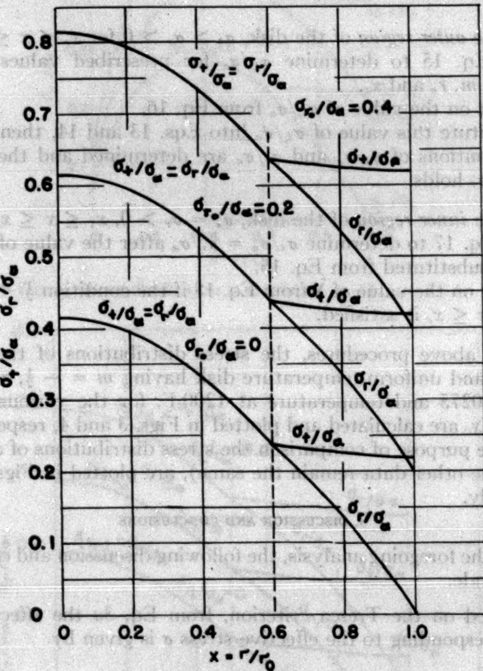

FIG. 6. Stress distribution in flat disk $m = 0$, $x_e = 0.6$.

4. There are two possible, extreme cases of the stresses distributions for variable-thickness disks (similarly for flat disks when $m = 0$ as

discussed in the preceding paragraph): If

(*a*) $\sigma_t > \sigma_r > 0$ at $x_i \leq x \leq 1$, then only Eqs. 13 and 14 are needed to calculate the stresses.

(*b*) $\sigma_t = \sigma_r > 0$ at $x_i \leq x \leq 1$, then only Eq. 17 is required for determining the stresses.

5. It is noticed in this creep analysis that based on the Tresca criterion and its associated flow rule, from the equilibrium equation, incompressibility equation and the stress-creep-rate relation the stress equations are derived in the simple closed form.

6. Experience shows that the values of the maximum tangential stress based on the Tresca criterion and its associated flow rule, on one hand, are considerably higher than the test data while the values predicted by the Mises criterion and its associated flow rule, on the other hand, are appreciably lower than the test data (2). It is felt that further spin tests of disks at elevated temperatures for various materials are needed before general conclusions can be drawn.

7.269
.960

Acknowledgments

The author wishes to express his appreciation to his colleagues in the Department of Mechanical Engineering, South Dakota State College and others for their cooperation in the preparation of this work.

REFERENCES

(1) B. M. MA, "A Creep Analysis of Rotating Solid Disks," JOUR. FRANKLIN INST., Vol. 267, pp. 150–165 (1959).

(2) A. M. WAHL, G. O. SANKEY, M. J. MARJOINE AND E. SHOEMAKER, "Creep Tests of Rotating Disks at Elevated Temperature and Comparison with Theory," *Trans. A.S.M.E.*, Vol. 76, pp. 225–235 (1954).

(3) M. B. MILLENSON AND S. S. MANSON, "Determination of Stresses in Gas-Turbine Disks Subjected to Plastic Flow and Creep," NACA Tech. Report No. 906, 1948.

(4) W. E. SKIDMORE, "Bursting Test of Rotating Disks Typical of Small Gas-Turbine Design," *Proc. Soc. Exptl. Stress Analysis*, Vol. VIII, pp. 29–48 (1951).

(5) A. M. WAHL, "Further Studies of Stress Distribution in Rotating Disks and Cylinders Under Elevated-Temperature Creep Conditions," *Trans. A.S.M.E.*, Vol. 80, pp. 243–250 (1958).

(6) C. R. SODERBERG, "Plasticity and Creep in Machine Design," Stephan Timoshenko Anniversary Volume, New York, The Macmillan Co., 1938, p. 198.

THE FRANKLIN INSTITUTE

MINUTES OF THE STATED MEETING

April 20, 1960

The Stated Meeting of The Franklin Institute was held at 8:15 P.M. in the Lecture Hall. Mr. J. G. Richard Heckscher, Executive Vice President, called the meeting to order with approximately 160 members and guests present.

Mr. Heckscher stated that the minutes of the February 17, 1960 Stated Meeting were published in the March issue of the JOURNAL. There being no corrections or additions these minutes were approved as published. The minutes of the March 16, 1960 Stated Meeting, he stated, would be published in the next issue of the JOURNAL and would be presented at a later meeting for approval.

Before presenting the speaker of the evening, Mr. Heckscher noted that tonight we were presenting the Eleventh Charles Day Lecture, which is an endowed lectureship established in June 1941 providing for lectures on engineering and science. Mr. Day was a member of The Institute from 1900, becoming a life member in 1910. He was a member of the Board of Managers from 1908 until his death in 1931 and a Vice President of The Institute from 1920 to 1923.

Mr. Heckscher then introduced Professor Stanley Keith Runcorn, Director of Physics Department, King's College, Newcastle upon Tyne, England, whose subject was "Rock Magnetism, Polar Wandering and Continental Drift."

Professor Runcorn's talk highlighted the most recent advances in the science of geophysics and in the course of his talk he used many slides of diagrams covering a broad phase of the subject and excellent color slides showing important and historical rock formation.

An interesting question period followed Professor Runcorn's talk, and the meeting was adjourned by Mr. Heckscher at 9:45 P.M., after he had expressed on behalf of The Institute our very deep thanks to Professor Runcorn for his inspiring talk.

WILLIAM F. JACKSON, JR.
Secretary

MEMBERSHIP

The following elections were approved on April 7, 1960 by the Membership Committee by authority given to it by the Board of Managers.

ANNUAL

Alice Jeanne Allen
Walter G. Arader
Earle W. Deppich
Henry Fagin
David E. Goode
Henry C. Guhl
F. M. Hakenjos
Martin J. Hesch
Arthur A. Holzbaur
William Honney
Charles C. Iden
Fred H. Kalesse
Otto Klima, Jr.
Stephen J. Koniers
Paul P. Kubik, Jr.
Leo D. Kushnir
Charles S. Landis
Robert A. Loscher
A. W. Martin
Charles A. McFadden
Charles G. Nicholson
Andrew J. O'Connell
Clemson N. Page
Susan Raefsky
Albert H. Redles
Harry Salem
Joseph Sauerwald
Charles A. Schehl
Walter R. Scott
William E. Scull, Jr.
Fredwood S. Shaw
George W. Shay
William E. Shoemaker
Morris Silver
Matti S. O. Siukola
James E. Sloan
John J. Smallwood
Roy H. Smiles
Gerald C. Smith
F. Russell Smith
James O. Stephens
E. Albert Wagner
Robert Rhamy Wagstaff
William S. Webb

EDUCATOR

Donald A. W. Blake
Lucie Kozikovski
Richard W. Stanford
William E. Stephens
Gino Tovazzi
Judith Wachstein

NON-RESIDENT

John A. Dienner

NECROLOGY

James Francis Cooke '36
Morris Llewellyn Cooke '12
Edwin K. Daly '49
Edward P. Loughran '57
John H. McClatchy '36
J. Aubrey McCurdy '41
Edward Woolman '95
Albert W. Zackey '50

BOOK REVIEWS

Electromechanical Energy Conversion, by David C. White and Herbert H. Woodson. 646 pages, illustrations, 6 × 9 in. New York, John Wiley & Sons, Inc., 1959. Price, $12.50.

The generalization of the analysis of electromechanical systems is a welcome feature of this book. In as much as we introduce the more intangible electromagnetic and electrostatic field theory, in the analysis of reactions, couplings and energy transfer from electric circuits to mechanical systems, the statement of suitable parameters or coordinators in the dynamical approach is important.

To be sure, the application of generalized coordinates to electromechanical systems and the use of Lagrange's equations are well known in the literature, but the authors have creditably extended its applications to many interesting problems, which hithertofore have been approximated by piecemeal circuit analysis.

In connection with the coupling reactions between electrical and mechanical systems, in place of the usual explicit introduction of mutual and self-inductance as coefficients describing the properties of the electromagnetic field, the authors have directly presented the parameters in terms of the flux linkages and the geometrical parameters and have extended the analysis to nonlinear electromagnetic systems, where the energy $\int i(\lambda, x)d\lambda$ or the co-energy $\int \lambda(i, x)di$ are utilized. In its application for computing electromechanical forces, the authors have carefully presented the distinction between these different forms.

In the authors' "Fundamental Relations in Electromechanics," the expression for D'Alembert's principle is confusing, if not incorrect. The concept of D'Alembert's principle is not postulated on the equilibrium of forces but rather on the equation of virtual work extended to the inclusion of the inertia forces. Its extension to dynamical applications, as with Lagrange's equation or in direct tensor form, is postulated on a choice of independent coordinates consistent with the constraints of the system. The authors' equation $\Sigma(\dot{p}_{ki} - f_{ki}) = 0$ evidently refers to a system of forces acting on the k^{th} coordinate, where $p_k = \Sigma p_{ki} = \Sigma m x_i \frac{\partial x_i}{\partial x_k}$. Now the generalized inertia force referred to the generalized coordinate x_k is $\Sigma m\ddot{x}_i \frac{\partial x_i}{\partial x_k}$ and not $\frac{dp_{ki}}{dt} = \frac{d}{dt}\left(m\dot{x}_i \frac{\partial x_i}{\partial x_k}\right)$, since $\frac{\partial x_i}{\partial x_k}$ is, in general, a function of the several independent or generalized coordinates of the system. Thus D'Alembert's equation should read $\Sigma m\ddot{x}_i \frac{\partial x_i}{\partial x_k} - \Sigma f_{ki} = \frac{dp_k}{dt} - \frac{\partial T}{\partial x_k} - \Sigma f_{ki} = 0$, where $p_k = \Sigma m\ddot{x}_i \frac{\partial x_i}{\partial x_k}$. Since $\Sigma m\dot{x}_i \frac{\partial x_i}{\partial x_k} = p_k$, the authors' equation $\Sigma \dot{x}_{ki} = 0$ seems meaningless. With nonholonomic systems the additional constraint reactions refer to condition relations $\sum_{(k)} A_k \dot{x}_k = 0$, for the assumed non-integrable coordinates defining the motion of the system.

Actually, the dynamical interpretation to closed circuits corresponds to generalized coordinates and the nature of the forces is quite different. Moreover, such coordinates are characterized as cyclic (or momentum) coordinates. Then in the equation $\frac{dp_k}{dt} - \frac{\partial T}{\partial q_k} = F_k$, the term $\frac{\partial T}{\partial q_k}$ should be deleted. The generalized force is $F_k = -\frac{\partial V}{\partial q_k} + f_{ki}$. Then we have n independent equations in the form $\dot{p}_k - F_k = 0$, for the n loops, where the couplings between the circuits may appear in any one of the terms, $\frac{dp_k}{dt}$ or $\frac{\partial V}{\partial q_{r_1}}$ or explicitly in f_{ki}. This gives a physical interpretation and not an analogy. It seems, therefore, unnecessary once the generalization is established, to introduce such terms as the inertia force of the kth node and the $\dot{x}_k$ velocity of the k^{th}

loop when circuit coordinates physically characterize the system.

Extending T to include the complete electromechanical system, then, since some of the coefficients of the electrical coordinates $\dot{q}$, may be a function of the mechanical displacement x, then $\frac{\partial T}{\partial x}$ accounts for the electromechanical forces. It should be pointed out that the *motional* emf's, dependent on the mechanical velocities $\dot{x}$, which are time derivatives of the coefficients with respect to x, of the momentum terms of the electric circuits, account for the electromechanical energy transfer and are of a gyroscopic nature, with respect to the electromechanical forces. These couplings disappear in the over-all energy equation. In like manner, the electrostatic capacity coefficients of q when a function of x then includes $-\frac{\partial V}{\partial x}$ for the electrostatic-mechanical forces, along with the elastic mechanical reactions; while $-\frac{\partial V}{\partial q}$ correspond to the capacity emf's for the electric circuits.

The authors state the Lagrangian $T-V=L$ as not sufficiently general to allow it to be extended directly to nonlinear systems. Actually, L applies to either linear or nonlinear systems, though not, without modification, to non-conservative systems.

A major theme of this book includes a study of coupling forces and the energy transfer between the electric circuit system and the mechanical parts with special reference to nonlinear relations of the parameters of the electrostatic or electromagnetic field systems. The electromechanical forces are expressed in terms of either the co-energy or energy form, where $f_e = \frac{\partial W_m'}{\partial x} = \Sigma_i \frac{\partial \lambda}{\partial x} - \frac{\partial W_m}{\partial x}$. With linear relations, these reduce to $f_1 = i_1 \sum_{r=1}^{n} \frac{\partial (M_{1r} i_r)}{\partial x_1} = i_r \frac{\partial \phi}{\partial x_1}$ between pairs of circuits i_1 and i_r with mutual inductance M_{1r} where $\lambda_{1r} = M_{1r} i_r$. The corresponding reactions on the electrical circuits are expressed in terms of the rate of change of the flux linkages. The field flux linkage is a function of both the current excitation and the mechanical displacement, where the latter is associated with the *motional counter emf* and the corresponding electromechanical energy transfer. The mutual coupling between circuits renders this method of approach particularly applicable to a matrix tabulation, that is, a tensor analysis of electrical machines.

The authors have extended this procedure to the analysis of various types of transducers and to generalized rotating machines, followed by specific applications to commutator machines and to a-c. machines as induction machines. In conjunction with the tabulation for complex rotating machine circuit analysis, the authors include some discussions on system dynamics and control analysis and corresponding block diagrams, with the analytical techniques as solutions by Laplace transforms.

In the authors' Generalized Rotating Machines a systematic analysis is developed through a well-defined grouping of windings. Two phase belts on stator and rotor with excitation are distributed sinusoidally at π electrical radians. The two phase belts are at quadrature. Arbitrary a^s and b^s stator magnetic excitation axes at quadrature are used as reference axes. The mechanical rotational angular coordinates ϕ establishes the phase relation of the rotor quadrature coil belts a and b. Obviously this can be extended to any number of phases ultimately reduced to quadrature phases. To arrive at the self- and mutual inductance coefficients between coils, it is necessary to establish the air gap flux distribution. This is calculated from the magnetic energy $W_M = \frac{1}{2}\int HBdv$ in terms of the circuit parameters $\frac{1}{2}\Sigma\Sigma L_{ij} i_i j_j$ where special consideration is given to pole saliency,

From this rotating machine configuration. the four circuit voltage equations, that is for the quadrature a and b phases of the rotor and stator, respectively, and the mutual torque in terms of the rate of change of the mutual flux linkages of the several circuits with respect to the rotor mechanical displacement ϕ. An interesting feature for the derivation of the latter is the use of the derivative of the over-all work equation, where the magnetic energy W_M is first stated in terms of the energy form and is reduced to its co-energy form $W_M' = \int \Sigma \lambda_j (i, \phi) di_j$. The method is also explicitly stated in its Lagrangian form, where the circuit and electromechanical coupling analysis are considered as a system.

Certain physical relations of the induction motor are compared with a fluid coupling. Actually, the relations are quite close. The working mediums are respectively the air gap flux or the fluid, which transfers the mutual torque between stator and rotor. The *slippage* energy $Ts \cdot \omega^s$ goes into heat through the I^2R losses in the rotor or in the heating of the fluid with the clutch. The torque reaction times the synchronous rotating field is equivalent to the counter emf times the stator currents, or to the authors' stator power (Eq. 3-239); and, with the clutch, this is its mechanical input from the drive shaft. These relations also concur with the authors' Eq. 3–237, where part of the slippage energy is transferred externally from the rotor circuit in the term $\breve{V}^r I^r \cos \theta'$. The potentiality of the induction motor as a "controlled" slippage clutch is great.

Undoubtedly the approach through tensor formulation of the interactions and energy transfer between complicated circuit systems is particularly adapted for computer methods, but such methods are limited in the over-all interpretation of the physical characteristics of electrical machinery. The concept for over-all approximations of field excitation, flux distribution, torque and power relation, in terms of distributed current excitation with stationary and revolving air gap waves; and the space phase relations of corresponding flux distributions, with ampere turns along the gap, in conjunction with various types of windings treated as over-all macroscopic parameters; permit equally important generalizations for various classes of machines with a physical picture of the interactions. This approach is particularly useful in a-c. machinery as with the induction motor. It is important to distinguish the air gap torque distribution and relations of space and time phase of the flux and counter emf's. The relations of various methods of excitation, armature reactions, with the above, are necessary for analytical design. The coordinating of these methods with the authors' tensor analysis would be an interesting undertaking.

It is to be noted the circuit equations and the electromechanical coupling forces can be established directly for the majority of examples listed. It is equally important to parallel a clear understanding of the nature of the reactions and energy transfer between circuits though a step-by-step build-up of the interacting electromagnetic forces and to distinguish directly the motional and transform emf's relating to the mechanical energy transfer and that to the field. Further, consideration should be given to the field excitation and flux build-up for the magnetic circuit and the gap distribution in relation to the electromechanical forces and hysteresis torque. This latter phase is one of the most difficult problems in the design of electromechanical systems.

From the reviewer's point of view, it would seem a more simplified approach of the simple basic characteristics, as to the nature of torque, current and flux, motional and transformer counter emf's, field excitation relations, rotating fields, etc., should precede the more ambitious program in the use of Lagrange's equations and such matters as quasi coordinates. The authors should note a large bibliography on the subject which deserves a careful scientific review.

The above is not suggested as a criticism of the authors' work, which enjoys an important contribution to the art, but rather as a criticism for a curriculum in teaching this subject.

Moreover, this book deserves special commendation in the development of a systematic and most interesting generalized analysis of electromechanical energy conversion systems.

Rupen Eksergian
The Franklin Institute Laboratories

Mechanisms and Motion, by K. H. Hunt. 114 pages, diagrams, 5½ × 8½ in. New York, John Wiley & Sons, Inc., 1959. Price, $4.25.

Since the subject of kinematics is an indispensible preliminary of such fields as dynamics of machinery and plastic deformation of frameworks, it is unfortunate that it should be so poorly treated by writers of engineering textbooks. Most such books contain such a mixture of vectorial dynamics, drafting room exercise, practical design limits and illustrations of mechanisms of varying complexity that the portion devoted to kinematics is often barely sufficient to justify the title.

While the writer of the present volume has made a laudable attempt (especially in the last few chapters) to present the abstract aspects of kinematics, from the point of view of the machine designer, his treatment of fundamentals can hardly be recommended. His discussion of so basic and important a concept as degrees of freedom, to which several pages are devoted, is quite hazy compared for example, to the brief and intuitively clear exposition in Sommerfeld's "Mechanics." Vector methods are discussed in one brief chapter which contains the erroneous statement that in plane motion, the relative centripetal and Cariolis components of acceleration are parallel, which is not true if the point in question has a radial component of velocity in the rotating coordinate system. The elaborate vector methods are hardly justified in the solution of extremely single examples in which the author fails to make clear an aspect of the Cariolis acceleration which e.g. Webster's treatment brings out; i.e., that it appears as the cross product in the expansion of the square of a sum. The author's solutions are thus quite unnecessarily complex especially in the case when the axes of rotation of the fixed and moving systems of coordinate are coincident.

The final chapters on space mechanics and advanced kinematics of plane mechanisms are more worthwhile, although the use of two-dimensional symbols for hinged guides in three-dimensional pictures does not contribute to clarity. A number of interesting mechanisms are shown in the problems.

KLAUS CAPPEL
The Franklin Institute Laboratories

PUBLICATIONS RECEIVED

MATERIALS AND TECHNIQUES FOR ELECTRON TUBES, by Walter H. Kohl. Revised edition, 638 pages, diagrams, 6 × 9 in. New York, Reinhold Publishing Corp., 1960. Price, $16.50.

FALLOUT, edited by John M. Fowler, with a foreword by Adlai E. Stevenson. 235 pages, diagrams, 6 × 9 in. New York, Basic Books, Inc., 1960. Price, $5.50.

INDUSTRIAL INSTRUMENT SERVICING HANDBOOK, by Grady C. Carroll. 848 pages, illustrations, 6 × 9 in. New York, McGraw-Hill Book Co., Inc., 1960. Price, $16.00.

ELECTRONIC COMPUTERS. PRINCIPLES AND APPLICATIONS, by T. E. IVALL. Second edition, 263 pages, illustrations, 5½ × 8½ in. New York, Philosophical Library, 1960. Price, $15.00.

AERONAUTICAL DICTIONARY, compiled by the National Aeronautics and Space Administration. 197 pages, diagrams, 5¾ × 9 in. Washington, Government Printing Office, 1960. Price, $1.75.

GERMAN-ENGLISH MATHEMATICS DICTIONARY, compiled and edited by Charles Hyman. 131 pages, 8½ × 11 in. New York, Interlanguage Dictionaries Publishing Corp., 1960. No price given.

MATHEMATICS REFRESHER, by Kurt Wolter. 96 pages, diagrams, 4½ × 7 in. New York, Philosophical Library, 1959. Price, $3.75.

ELEMENTARY MODERN PHYSICS, by Richard T. Weidner and Robert L. Sells. 513 pages, illustrations, 6 × 9 in. Boston, Allyn and Bacon, Inc., 1960. Price, $8.50.

DATA BOOK FOR CIVIL ENGINEERS. DESIGN, by Elwyn E. Seelye. Third edition, Volume 1, v.p., illustrations, 9 × 11½ in. New York, John Wiley & Sons, Inc., 1960. Price, $24.00.

BOOK NOTES

Vacuum Processing in Metalworking, by J. Wesley Cable. 202 pages, illustrations, 5 × 7½ in. New York, Reinhold Publishing Corp., 1960. Price, $5.50.

In this small text the relatively new field of vacuum technology receives complete and practical treatment. It also encompasses a wide range of operations in the metalworking field. The general phases of vacuum technology such as the means of producing low pressures and their measurement is reviewed. The author's aim is to present vacuum technology in a descriptive manner, rather than in a highly technical form. As a result, it is beneficial to any industry involved in the refining and processing of metals.

Rocket Propellant Handbook, by Boris Kit and Douglas S. Evered. 354 pages, diagrams, 6¼ × 9¼ in. New York, The Macmillan Company, 1960. Price, $12.50.

Nearly a hundred chemicals having possible use as rocket propellants are described in this concise handbook. The chemicals include fuels, oxidizers, and monopropellants. Tables are included giving such data as heat value, density at various temperatures, specific impulse and performance with alternative oxidizers or fuels. The text will be of interest not only to the rocket propulsion industry and the military services, but also to the chemical industry, manufacturers of handling and storage equipment, and engineering companies involved in the design and construction of facilities.

Aircraft and Missile Design and Maintenance Handbook, by Charles A. Overby. 369 pages, diagrams, 6 × 9 in. New York, The Macmillan Company, 1960. Price, $9.75.

A practical handbook for mechanics, inspectors, draftsmen, supervisors, designers and modification engineers. Containing over 160 tables and 40 figures to illustrate the standard methods of equipment installation and maintenance, the book gives standards and hundreds of tips on the proper handling of materials and tools. Topics covered are electrical and plumbing systems, materials of construction, aircraft and missile hardware, color codes and conversion systems, and processes such as metal spraying, anodizing, rust-proofing, plating, welding and brazing.

Elements of Ion Exchange, by Robert Kunin. 164 pages, diagrams, 5 × 7½ in. New York, Reinhold Publishing Corp., 1960. Price, $5.75.

This little book provides a basic understanding of ion exchange techniques, written specifically for those with little or no theoretical background. As there is scarcely an industry today in which ion exchange is not involved, this concise handbook, giving the description of its development and importance, will be of valuable assistance to executives and operating personnel. In addition, a broad view of the subject is provided for analytical, physical and industrial chemists, biochemists, agronomists and nuclear researchers.

The Aerodynamics of Powered Flight, by Robert L. Carroll. 275 pages, diagrams, 5¾ × 9 in. New York, John Wiley & Sons, Inc., 1960. Price, $8.50.

The author gives a new approach to the subject, both simple and direct. By showing that lift is directly dependent on power and by treating rocket power as the logical lift source, the book provides an exposition of the science and mechanisms of powered flight that is unique in its clarity and simplicity. A foundation in fluid flow and airfoil theory is detailed, while also introducing the fundamentals of propulsion, stability, performance, design and control. In order to emphasize the practical aspects of flight, 216 problems are included.

PETROLEUM ENGINEERING: DRILLING AND WELL COMPLETIONS, by Carl Gatlin. 341 pages, diagrams, 8½ × 11 in. New York, Prentice-Hall, Inc., 1960. Price, $13.00 (trade edition); $7.95 (text edition for classroom adoption.)

The technical as well as non-technical reader will find this book useful as a reference and practical for self-study of the problems of drilling and completing oil wells. The author examines the basic elements of drilling, testing, formation, evaluation and completions, also surveying various geological and geophysical exploration methods. An extensive bibliography, listed by chapters is an excellent guide to special topics. Illustrations combined with an uncluttered text provide a clear, readable coverage of well location and development.

ACRYLIC RESINS, by Milton B. Horn. 184 pages, illustrations, 5 × 7¼ in. New York, Reinhold Publishing Corp., 1960. Price, $4.50.

This little handbook in the Plastics Applications Series, describes the four types of acrylics in respect to their manufacture, fabrication and applications. These types include cast products, molding compounds, emulsion and solution compounds. The author explains raw materials and manufacture of these polymers, then he covers the current and future developments in terms of potential use in a great variety of products. Thus, a complete guide is given to chemists, sales personnel and executives on every aspect of acrylics in addition to a broad understanding of uses and future trends.

PHYSICS: FOR STUDENTS OF SCIENCE AND ENGINEERING, by Robert Resnick and David Halliday. 554 pages, diagrams, 6 × 9¼ in. New York, John Wiley & Sons, Inc., 1960. Price, $6.00.

The authors have aims to reveal the unity of physics in many ways throughout this text. For example, the conservation laws of energy, linear momentum, angular momentum, and charge are used repeatedly. Wave concepts and properties of vibrating systems, such as resonance, are used in mechanics, sound, electromagnetism, optics, atomic physics and nuclear physics. The field concept is applied to gravitation, fluid flow, electromagnetism and nuclear physics. The mathematical level of the book assumes a concurrent course in calculus. An unusually large number of worked-out examples, with the "plug-in" variety used only to emphasize a numerical magnitude. Algebraic, rather than numerical solutions are stressed. The mks system of units has been adopted throughout the text, although the British engineering system is also used in mechanics.

CURRENT TOPICS

Tiny Microphones Record Space 'Hits'.—The 142-lb. Explorer VI satellite is carrying two tiny microphones as part of a micrometeorite detection experiment sponsored by the Air Force Cambridge Research Center (AFCRC), Bedford, Mass. AFCRC is an Air Research and Development Command (ARDC) facility.

Explorer VI, launched August 7, 1959, circles the Earth at an estimated 22,000 mph. Its orbit was programmed for 23,000 statute miles at apogee (farthest point from Earth) and 160 statute miles at perigee (closest point to Earth). Scientists estimate the satellite's life span at two years.

Purpose of the instruments is to measure the number of times the "paddle wheel" satellite, launched under the direction of the National Aeronautics and Space Administration (NASA), is struck by these tiny particles in space.

The microphones, located opposite each other, are firmly mounted in the center of 6-in. by 12-in. strips of the satellite's $\frac{1}{16}$-in. thick aluminum skin. They detect either a strong or weak hit by particles one micron (a thousandth of a millimeter) in diameter or larger. More than 25,400 microns placed side by side would measure but a single inch.

One of these dust particles striking the satellite's surface generates an acoustical pulse which, after traveling through the exposed plate, is transformed by the microphone into an electrical pulse. This electrical pulse is in turn transmitted to data accumulating stations on Earth. Size of the particles is determined between certain known limits from the magnitude of the pulses generated.

Thermocouple Measures Temperatures of Molten Metal.—A new expendable immersion thermocouple for measuring molten metal temperatures has been developed by the Instruments and Systems Division of Engelhard Industries, Inc., Newark, N. J. Primarily designed for measuring steel temperatures in both open hearth and electric furnaces, it may be used with equal efficiency with other molten metals. The new unit combines improved economy, faster response, high accuracy and simplified assembly.

The expendable thermocouple design is simple consisting of a ceramic base which serves as a mounting for the noble metal thermocouple wires. A firmly anchored transparent fused silica tube protects the thermocouple wires and is, in turn, protected from slag and floating solids by a special metal cap. The cap absorbs the physical shock of immersion and melts away immediately after it has plunged beneath the slag.

Special design of the thermocouple unit and its receptacle allows the unit to be assembled without requiring alignment of contact pins. Design also assures that molten metal cannot penetrate the assembly and damage the plug receptacle.

Two different thermocouple combinations are available in the Engelhard unit, either platinum *vs.* platinum 10 per cent rhodium or platinum *vs.* platinum 13 per cent rhodium.

Standard pipe, handle and lead wire assemblies may be used with the unit or these components may also be obtained from Engelhard.

V.2
196

Glass Fibers Used in Concrete.—A method of producing concrete structural elements both reinforced and prestressed by glass fibers has been developed by the U. S. Army Engineer Research and Development Laboratories, Fort Belvoir, Va. The method, which has been patented, was developed by Mr. Solomon Goldfein, a chemical engineer, who is chief of the Plastics Section in the Materials Branch of the Laboratories.

It is expected to be used in special applications, where the light weight, corrosion resistance, absence of magnetic field, and electrical resistance of the reinforcement are important factors to be considered. It has been considered for such structures as piling for docks exposed to salt water, concrete ships and vehicles requiring non-magnetic reinforcement, structures where the reinforcement must not be allowed to conduct electricity, and as reinforcement for large concrete pipes conducting water.

One of the major difficulties experienced in producing such structural elements has been the problem of securing adequate bond of the glass fibers to concrete. The method developed by the Laboratories solves this problem through the use of a binder, such as an epoxy resin, specially formulated, which bonds the glass fibers to themselves and to the concrete, thus protecting them against the high alkalinity of the cement.

The reinforced concrete may be made by several different methods. In one method, a prefabricated plastic glass fiber rod having a silicious or cementitious covering on its surface, is used. The rod is embedded in concrete exactly as its steel reinforcement counterpart. The covering acts to increase the strength of the bond between the glass fibers and concrete. In the other method, glass fiber impregnated plastic embedded in the concrete hardens during the setting of the concrete, thus effecting a bond.

Prestressed and poststressed concrete may be made by using principles established previously during the development of prestressed plastics by Goldfein. The rods may be prefabricated with special gripping devices bonded to them for tensioning.

The material probably will never compete in ordinary building construction, because of its low modulus and high cost compared to steel. The former disadvantage, however, is expected to be considerably reduced soon by the use of a special glass fiber, which has a modulus almost equal to that of steel.

In countries having no iron resources but plenty of glass-making raw material, the price differential will lose some of its significance.

Leveling Agent Improves Dyeing.—Deeper, level and solidly dyed shades on wool and/or nylon stocks, yarns or fabrics can now be obtained economically with neutral dyes by using a new leveling agent developed by American Cyanamid Company.

Known as Calco Leveling Salt LV, the agent is applied with the dye under processing conditions, pH 4–6, that should be used for neutral dyes. The soft hand of wool is retained and the striped or Barré effect encountered in dyeing nylon carpeting is eliminated. This salt is also expected to solve similar problems in dyeing such other forms of nylon as hosiery and sweaters.

Unlike other leveling agents, Calco Leveling Salt does not act as a retarding agent, which makes incomplete exhaustion of the dye bath the penalty of satisfactory appearance. Cyanamid's new agent allows the colorant to dye rather than stain the cloth. As a result, shades may be matched by adding color in process, a procedure not possible with other agents of this type.

Calco Leveling Salt LV serves the dual purpose of wetting out the fiber and controlling the dyeing. Its use does not have any adverse effect on the fastness properties of the dyes used.

Improved Rubber Gaskets.—American Felt Company, Glenville, Conn., has announced the introduction of "Vistex III," a new and improved fiber-reinforced nitrile rubber gasket material. The new material, made of synthetic fiber-reinforced "Teflon," is recommended for its excellent stability to corrosive gases and liquids under both high and low temperature conditions.

Among features claimed for the new "Vistex" are its 100 per cent compression recovery, its exceptional tensile strength, its resistance to oil and aromatic fuels, good flexibility, and its non-adhesive and non-corrosive properties.

"Vistex III" is available in sheet form, up to 30 in. × 60 in., and in standard $\frac{1}{8}$, $\frac{1}{16}$, $\frac{1}{32}$, $\frac{3}{32}$ and $\frac{1}{64}$ thicknesses. It has 84 lb. per cubic ft. density and a minimum tensile strength of 1000 psi. At 300° F., it retains 620 psi. tensile strength and at 430°, loses only 105 psi. It is especially well suited for gaskets where light weight is a factor. One square yard of $\frac{1}{32}$ "Vistex" weighs only 30 oz.

The new material can be precision cut or punched into gaskets, strips or washers. It has excellent chemical stability to acids, alkalis, aliphatic and aromatic compounds. Among operating characteristics found to be inherent in the new material are excellent die and hand-cutting properties, freedom from fraying and raveling, and minimum-pressure sealing on either polished or irregular surfaces.

Under most conditions, it can be re-used. It has very high tear value and because of its high strength, it is an ideal industrial gasket material.

Because of its high degree of chemical stability, and the versatility of uses, it is believed AFCO's new "Vistex III" will find wide application in a variety of industrial uses.

The Ferreed.—A team of engineers at Bell Laboratories has invented a very fast electromechanical switch called the "ferreed." It utilizes a new technique for actuation which is compatible in speed with electronic circuits.

The ferreed may find use as an interconnecting element in telephone switching networks, where it could be controlled a thousand times more rapidly than switches presently employed.

Inventors of the new switch, A. Feiner, C. A. Lovell, T. N. Lowry, and P. G. Ridinger, are members of the technical staff of Bell Telephone Laboratories. They anticipate applications for the ferreed in various types of systems where advantage may be taken of metallic contacts controllable by current pulses of a few microseconds duration.

Magnetic materials that can be quickly switched between two alternate states have been widely used as "memories" for storing information in digital computers. The useful output from these elements has generally been limited, however, to electrical signals of a transistory character.

In conventional electromagnetic relays, on the other hand, continuous electrical currents can be used to open and close metallic contacts for extended periods of time, but at speeds limited by the mechanical motion of the moving parts.

The ferreed combines the rapid

switching of bistable magnetic material with metallic contacts for output indications that persist as long as desired without further application of power. In several models of the device, a cobalt ferrite has been used as the magnetic material and a glass-sealed magnetic reed switch for the output contacts—hence the name, "ferreed."

In operation, the magnetic material is switched by a magnetomotive force applied, typically, as a five-ampere current pulse in a thirty-turn winding. Control pulses as short as five microseconds will switch the magnetic material, resulting in the passage of magnetic flux through the movable members of the reed switch. Actual closure of the contacts is delayed by inertia of the reeds for several hundred microseconds.

Release of the contacts is brought about by cancellation of the magnetic flux through the reeds, as the result of another five-microsecond switching operation. Opening of the contacts requires less time than the closing operation.

Several new magnetic materials have been synthesized for use in developmental models of the ferreed. Among these are ferrites exhibiting characteristics midway between permanent magnets and computer memory materials, and ferrite suspensions in plastic "tailor-made" for specific magnetic, electrical, and mechanical properties. The reed switch is similar to a type used in standard electromagnetic relays for the past decade.

In a telephone switching network, subscribers are interconnected by the closure, in specified patterns, of switches called "crosspoints." A typical central telephone office contains many thousands of these switches; of these, a few dozen are operated for each call. Those crosspoints required for a particular connection must be selected by the coincidence of pairs of control pulses. The ferreed's magnetic structure responds to a pair of pulses by closing the output contacts. They are opened by a subsequent single pulse.

Besides coincident pulse operation and rapid actuation, the magnetic structure permits the desired switching by current pulses of widely variable character.

The result, when ferreeds are used in switching networks, is reliable operation from simple control circuits.

Fifteen-Story Missile Tower.—A 15-story high portable missile service structure, believed to be the tallest and heaviest pneumatic tire-mounted structure in this country, has been developed for use at missile test sites, according to a recent Department of the Army announcement.

The portable service tower was developed by the U. S. Army Engineer Research and Development Laboratories, Fort Belvoir, Va., for use in servicing missiles of the Redstone and Jupiter classes, or any missile up to 136 ft. tall. The tower was designed and built by the Noble Company, Oakland, Calif.

Previous missile towers have been either fixed or rail-mounted. The new 151-ft., 350,000-lb. structure, however, is mounted on two base trailers of six wheels each. The outboard rearmost wheels are driven by an electric motor, and front wheels are steered by hydraulically operated cylinders controlled by an electric sensing device running on a steering track.

After being positioned, the two crane hooks operating from the "hammerhead" top pick up the missile and set it on its launcher. Jack pads are lowered and the structure is off tires until the time for roll back.

The tower has six adjustable platforms for use by engineers and scientists in preparing a missile for flight. It also has two elevators, a complete intercom system, and a "panic button." The button is designed for use at the most critical moment of missile fueling. If a fire should start, a push of the button, either on the tower or in the control bunker, slides the platforms back from around the missile, lifts up the jacks off the ground and wheels the tower itself away from the fire.

An engine-generator, motor-generator, hoists, motors, gear boxes, and electric control panels are mounted on the base trailers. The twin masts can be taken apart and the flat panels and platforms stacked on transport trailers for movement by aircraft, or for highway tow.

Solid State Data Processing System.—The solid state IBM 7080 data processing system has been announced by International Business Machines Corporation. It is the most powerful computer yet designed specifically for business with processing speeds up to ten times faster than the IBM 705 systems.

The 7080 is capable of producing management reports and processing payrolls, inventory control, billing and similar accounting jobs at a substantially lower job cost than the previous systems.

New design advances that give the 7080 its high capacity include: (1) fastest memory available, called Communication Storage, which can transfer information between tape units and main data storage so fast (1.09 microsecond character rate) that up to five tape units can be reading in or out simultaneously; (2) a main memory from which any of up to 160,000 characters of information can be called into the central processing unit in 2.18 microseconds giving the 7080 the fastest main storage available; and (3) priority processing, a system which achieves maximum efficiency of simultaneous reading, writing and processing operations, permits input/output devices to automatically control the flow of programs.

A typical 7080 system will sell for $2,528,000 or rent for $55,500 a month. This includes the central processing unit, magnetic core storage, console, two tape control units and twelve magnetic tape units. A basic system will sell for $2,233,000 or rent for $49,100 a month.

The new concepts in the 1.09 microsecond communication storage simplify the attachment of input/output devices and provide the basis for the priority processing system.

As a result, the 7080 can take in or feed out information to or from sources such as its magnetic tape units, process and transmit data internally, all at the same time. Combined with priority processing, this greatly reduces job times.

In one second, the 7080 can: read or write 312,500 characters of information; make 303,000 logical decisions; add or subtract 78,000 six-digit numbers; multiply 7,100 six-digit numbers.

The 7080 has a unique, newly-designed console which includes a digital display of registers. This information is projected in back-lighted Arabic numbers for easy reading by the operator. Previously, this information appeared on systems' consoles in the form of binary-coded lights.

The 7080's increased main memory speed of 2.18 microseconds compares to seventeen microseconds on the IBM 705 I and II systems, and nine microseconds on the 705 III. A

V.2
196

magnetic core memory of either 40,000, 80,000 or 160,000 characters is available on the new system. The 705 I has a storage of 20,000 characters, the 705 II has 40,000 and the 705 III has an 80,000 character storage.

Ultra high-speed access to memory in the 7080 significantly contributes to stepped-up computing. The 7080 is designed to accept 705 I and II programs and internally process them ten times faster, and 705 III programs six times faster. Even greater speeds can be realized when 705 programs are modified to take advantage of the increased power and flexibility of the 7080's new program instructions.

The new system has three modes of operation—705 I and II, 705 III and 7080. The operator can establish either 705 mode simply by pushing a compatibility switch on the console.

Major 705 programs which will operate on the 7080 system include Autocoder III, Input/Output Package, Decision Making Language, FORTRAN, Report Generator, File Maintenance System, 705 Processor, Utility Programs and Sort and Merge Routines.

The solid state 7080 needs only fifty per cent of the air conditioning and power of its predecessors, and thirty per cent less space. These reductions will permit expansion of a solid-state system within present facilities as capacity requirements grow.

Even greater savings can be attained if peripheral tube equipment is replaced with the solid state IBM 1401 system. Complete tape and tape unit compatibility is achieved between on-line and off-line equipment because the 729 II and 729 IV tape units are used in both systems.

With 1401 off-line printing, punching and card-to-tape conversion equipment, the 7080 becomes a powerful system for applications such as demand deposit accounting and other banking operations; railroad freight car accounting; public utility customer accounting and merchandise control in the retail industry.

Fluoroscopic Screen Detects Presence of Stray Radiation.—A new-type fluoroscopic screen called RAD-A-LERT which enables radiologists to detect unabsorbed stray radiation, has been announced by United States Radium Corporation. A patent has been applied for. The new screen—which provides this extra measure of safety and service to the radiologists—features a special border, a portion of which fluoresces red, in contrast to the yellow-green of the screen proper. This red signal indicates to the radiologist that radiation is escaping beyond the protective lead glass of the fluoroscopic assembly.

The radiologist can immediately take steps to remedy this condition through reduction of shutter openings, altering patient-screen distance, proper tube centering or other corrective measures.

In actual use, the border of the RAD-A-LERT screen presents a level of brightness readily visible, yet not sufficiently bright to disturb dark adaptation or interfere with continuous fluoroscopy.

High-Speed Silicon pnpn Diode Switch.—A silicon pnpn diode capable of switching at extremely high speeds was described in a paper presented at the Winter General Meeting of the American Institute of Electrical Engineers. The switch, developed at Bell Telephone Laboratories, was a result of the joint efforts of A. N. Baker, J. M. Goldey, and I. M. Mackintosh.

This device is useful in switching moderate amounts of power with extreme rapidity. Typical applications are in line pulsers, and high-speed gates for use in certain types of telephone equipment now under development. Turn-on time is approximately ten millimicroseconds and turn-off time is about the same, including the storage time of the charge carriers—which is around 4 millimicroseconds. More refined measurements show that current is down four orders of magnitude in less than 100 millimicroseconds. Several watts of power can be switched by this device.

The diode has a triple diffused structure, starting with a wafer of n-type silicon. The wafer is then etched to form a mesa-type construction to reduce the area, resulting in a unit having a capacity of about 5 micromicrofarads.

High-speed operation is achieved by the use of thin base layers and by reducing the lifetime of the charge carriers. The latter can be done very precisely either by irradiating the device with high-energy electrons or by diffusing in minute amounts of gold.

In the "on" condition, this diode has a resistance of about 2 ohms. Impedance when "off" is represented by a capacitance of 5 micromicrofarads with an extremely low leakage current of around a millimicroampere at room temperature.

Undersea Arctic Cable.—An important link in the rearward communications for America's Ballistic Missile Early Warning System (BMEWS) became a reality recently when the first undersea telephone cable above the Arctic Circle was completed. Owned by the United States Air Force, it connects Air Force installations in Greenland and Canada.

The Arctic undersea cable operation was carried out under the direction of the Western Electric Company with the cable placing being handled by the Long Lines Department of the American Telephone & Telegraph Company. Western Electric is responsible to the United States Air Force for the design, installation and testing of rearward communications routes for America's BMEWS project.

Four nations—Canada, Denmark, Great Britain and the United Srates—combined to make this first telephone cable beneath Arctic waters possible.

This undersea cable which incorporates built-in amplifying repeaters spaced some 40 miles apart, provides reliable, time-tested communication channels between the United States Air Force Base at Thule, Greenland and other military stations in northern Canada. It is similar in construction to the existing transoceanic telephone cables and will be used for military purposes. Work on the cable started in the summer of 1958 and was completed late in 1959 at a cost of about $9,000,000.

It was "touch and go" as to whether the cable would be completed on schedule because of two factors: the relatively short periods of the year when the Baffin Bay and Davis Strait region would be free of pack ice and icebergs, and the fact that no one had ever placed an undersea telephone cable in Arctic waters.

In addition, an emergency developed—one with possible serious consequences for the cable project—in June of last year the British cable ship *Ocean Layer* was gutted by fire while completing the second transatlantic cable. The *Ocean Layer* had been scheduled to lay the second of the twin 700-mile BMEWS cables. The first cable had been put down successfully the summer before by the British Post Office cable ship, HMTS *Monarch*. To surmount the emergency, two vessels, the American Cable and Radio Corporation's cable ship *John W. Mackay*, and the United States Military Sea Transport Service cargo ship *Lt. James Robinson*, worked as a team.

The *Mackay*, when fully loaded, carried only enough cable to reach approximately half the distance from Cape Dyer to Thule. The other ship was used to re-supply her. The *Robinson* was converted from a standard cargo ship to a cable carrier by around-the-clock shifts of workers at an east coast navy shipyard.

The *Mackay* loaded cable at the Simplex Wire and Cable Company docks in Newington, New Hampshire in late August then sailed to Cape Dyer, on Baffin Island, and began laying cable northward toward Thule. Meanwhile, the *Robinson* loaded the remaining lengths of the needed cable and sailed directly to Thule. When the *Mackay* completed laying the first segment of the cable she buoyed the cable end and sailed for Thule.

There, she reloaded her cable tanks from the *Robinson*, then raced back down Baffin Bay until she located, picked up, and spliced into the buoyed end of the cable. The *Mackay* then continued northwards to Thule, laying the last segment of the second cable. Several days later she reached there and spliced her cable into the shore end.

The first undersea telephone cable in Arctic seas had become a reality—ahead of schedule.

YOU CAN ADVANCE SCIENCE EDUCATION

Today, more than ever before in its 135-year history, there is vital need for The Franklin Institute to effectively promote education in science and technology. It is imperative that we meet this challenge by providing adequate educational opportunities in these fields. This requires vision, objective planning, and money. We have more than enough of the first two requisites, but far too little of the third.

Our programs are aimed at professional scientists and industry, as well as the lay public and young people seeking inspiration and guidance in choosing a career. The Institute's educational programs are impressive, for they begin with students in the early grades of our elementary schools and continue throughout an individual's professional or industrial life. With more funds at our disposal, the scope and vigor of these activities could be greatly increased.

The Franklin Institute is not richly endowed. It is a non-profit organization, depending for encouragement and support on an understanding public. Capable and conservative management assures wise administration of all funds.

Your gift or bequest, large or small, will be deeply appreciated and will be used effectively to broaden the Institute's educational usefulness. There is a warm satisfaction in giving financial support to an organization that has pioneered in, and is dedicated to, the advancement of science and technology through education.

When property is transferred, title should be in the name of The Franklin Institute of the State of Pennsylvania for the Promotion of the Mechanic Arts.

The Secretary of The Franklin Institute will gladly furnish you with additional information. Write to him at The Franklin Institute, Benjamin Franklin Parkway at Twentieth Street, Philadelphia 3, Pennsylvania.

NATIONAL BUREAU OF STANDARDS NEWS

CONTINUOUS-PRODUCTION VACUUM FURNACE

A continuous-production vacuum furnace[1] for evacuating and sealing ceramic wafer electron tubes[2] has been designed by the National Bureau of Standards for the Navy Bureau of Aeronautics as part of the Navy's industrial preparedness program. Mechanical development and construction of the furnace were undertaken on contract by Sanders Associates, Inc., Nashua, N. H.

With this system, the tube assembly is introduced into a vacuum and heated to a high temperature. The combination of heat and vacuum degasses the tube, and the high temperature brazes together the metallized surfaces of the ceramic wafers to make a hermetically sealed unit.

The machine was conceived and designed by C. P. Marsden of the Bureau's electron devices laboratory in connection with a study of industrial processes suitable for fabricating electronic components.[3] The automatic production methods for ceramic wafer tubes required processing the assemblies into completely sealed and ready-to-use units by evacuating, degassing, and sealing in a single continuous operation. The vacuum furnace performs these operations with control of only temperature, degree of vacuum, and time of processing. The high temperature eliminates the need for getters, thus simplifying tube design. The furnace has been used to produce up to 200 tube assemblies an hour.

Essentially, the vacuum furnace is a vertical tube, about 11 ft. long, of heat-resisting alloy, surrounded by a heating unit, and open to the atmosphere at both ends. Through this tube passes a series of hollow cylindrical specimen carriers, each separated by a short piston fitting closely inside the tube. These parts are introduced into the top of the tube at atmospheric pressure; once inside, they are evacuated through ports along the side of the tube and through holes in the carriers. The pistons and carriers pass through the tube under gravity feed. In the prototype model, the sliding fit of the pistons maintains the vacuum at 10^{-5} mm Hg, and the central portion of the tube can be heated to 1000° C. After processing, the parts are removed from the lower end of the tube at atmospheric pressure and at reduced temperature.

With the carrier loading and unloading equipment the machine requires about 15 ft. vertically. A 15-ft. square of floor area is adequate for the vacuum pumps, controls, and other associated equipment.

The central 7-ft. portion of the tube is surrounded by the electric heating element. This element is simply resistance wire supported in the inner side of a grooved ceramic cylinder. Five heat reflecting shields surround the heating unit; the inner two are of molybdenum, the outer three of stainless steel.

V.2
196

---

[1] Patent No. 2,894,795, "Automatic Evacuation System for Vacuum Tubes," awarded to C. P. Marsden, 14 July '59.

[2] "Ceramic Wafer Tubes for Modular Units," by C. P. Marsden, *Electronics*, Vol. 32, No. 39 (Sept. 25, 1959).

[3] "Project Tinkertoy," *NBS Tech. News Bul.*, Vol. 37, p. 11 (1953).

The carriers, 2 in. in diameter and about 4 in. long, are of alloy steel and fit closely inside the tube. They contain a number of $\frac{1}{2}$-in. holes to permit escape of gas. The outside bearing surfaces of the pistons are flame-coated with tungsten carbide to prevent the bare metal surfaces from brazing together in the intense heat of the furnace section. This coating is extremely hard; after the machine had been used continuously for 6 months, the coated surfaces showed negligible signs of wear.

Several vacuum pumps are employed to reduce the air pressure near the ends of the tube and to maintain a high degree of vacuum in the central heating section. Relatively little air leaks into the system past the carriers and pistons; the air removed from the central section is mostly that desorbed from the surfaces of the parts entering the system.

A similar machine could well be devised for continuously processing devices other than ceramic radio tubes. The coating of lenses or resistors by vapor-plating, and the production of vacuum condensers and switches are possible applications. Where the processed article must come out of the vacuum near room temperature, the lower end of the furnace could be lengthened and water-cooled.

DESIGN OF CORNER REFLECTOR ANTENNAS

A design analysis of corner-reflector antennas has been carried out by the National Bureau of Standards Boulder (Colo.) Laboratories under the sponsorship of the U. S. Air Force. The results of this evaluation [4] by H. V. Cottony and A. C. Wilson of the Bureau's Central Radio Propagation Laboratory provide comprehensive and detailed information on designing high-performance, economical corner reflectors.

A corner-reflector antenna consists simply of two plane reflecting surfaces joined edge to edge to form a corner, which is usually parallel to the ground. The driven element is placed in the aperture between the two planes. This type of antenna has the advantages of high gain, broad frequency response, narrow beam width, low back radiation, low cost, and ease of construction.

Early experimental work in ionospheric scatter propagation stimulated interest in corner reflectors because they are particularly suitable for this mode of communication. Even though these antennas had been used prior to the new experimental scatter circuits, their performance was known only qualitatively. Therefore as part of its propagation research program, the Bureau undertook an investigation of corner deflectors to determine how gain varies with changes in width and length of reflecting surfaces, angle of aperture, and position of driven element.

The experimental corner-reflector antenna used for this investigation consisted of two lattice-type wooden frames, each 12.3 ft. (five wavelengths at 400 mc.) wide by 12.3 ft. long, supporting the reflecting surfaces. The reflectors were of overlapping strips of sheet aluminum fastened to the frames so that removal of one strip would subtract 0.2 wavelength from the surface.

---

[4] "Radiation Pattern of Finite-Size Corner-Reflector Antennas," by A. C. Wilson and H. V. Cottony, *IRE Trans. Ant. & Prop. AP-8*, No. 2, March 1960; for further technical information, see "Gains of Finite-Size Corner-Reflector Antennas," by H. V. Cottony and A. C. Wilson, *IRE Trans. Ant. & Prop.*, Vol. AP-6, No. 4, October, 1958.

Width could be varied by trimming the lengths of the strips. The two frames were pivoted along the same axis, and the angle of aperture could be varied from 20 to 180°.

The driven element was a folded half-wave dipole. Its position could be varied from 0.07 to 2.5 wavelengths from the apex of the reflecting surfaces. The dipole's support also served as a balun to transform the impedance of the system to about 50 ohm. Fine adjustment, for an exact match to a 50-ohm line, was provided by a two-stub tuning unit. Gain was measured at 400 mc by comparing the system with a known antenna.[5]

Although in practice collinear arrays of four and more dipoles are used in scatter antennas to obtain gains of over 20 db, the general performance can be predicted from an experimental system using only a single dipole. Therefore, only the single dipole was used for the measurements.

Results of the measurements indicate that minimum reflector width is 0.5 wavelength for the smallest usable value of gain. With an increase in width up to 2 wavelengths, gain increases. However, beyond this, there is little or no increase in gain, and under some circumstances it may actually decrease.

For maximum gain, the dipole must be in one of several discreet positions—referred to as first, second, third, etc., in order of distance from the apex. The exact location of each position is a function of the aperture angle.

When the dipole is in the first position, gain increases monotonically as reflecting surface length increases. When the dipole is in the second or third positions, the same relation holds true generally, except for surface lengths less than 1.5 wavelengths. For these shorter lengths, the relation is not only too irregular for simple analysis but also does not provide the antenna designer with any useful data.

Maximum gain along the forward axis seems to be achieved with the dipole in the second position. In this case, the reflecting surface should be more than two wavelengths long and approximately two wavelengths wide.

Ionospheric scatter antennas designed for the lowest portion of the VHF band should have especially low secondary lobes and minimal radiation to the rear, as radiation in these undesired directions is likely to result in self-interference from multi-path propagation. An important advantage of the corner reflector over other types of antennas is that it can be designed to have extremely low back radiation. The small amount that does occur results from diffraction around the edges and from penetration through small openings in the reflector surfaces.

Radiation patterns have been compiled for a variety of sizes of corner reflectors.[4] This material has been further summarized graphically so that beam widths and back radiation levels for any combination of surface lengths and widths are easily determined.

---

[5] "Techniques for Accurate Measurement of Antenna Gain," by H. V. Cottony, NBS Circ. No. 598. Available from the Superintendent of Documents, U. S. Government Printing Office, Washington 25, D. C. Price, 15 cents.